CHAPTER 4

4. RESULTS AND DISCUSSION:

This work is concerned with preparation and characterization of nanocomposite fibers suitable for use as catalyst. Effort has been made to prepare and use copper oxide/cerium oxide (CuO/CeO_2) nanofibers for this purpose. Various compositions of CuO/CeO_2 composite nanofibers and pure CeO_2 have been characterized and tested for their catalytic activity, morphology, elemental composition; surface, structural features, thermal stability and details of the results of characterization, stability of all prepared catalysts and catalytic activity are given in the following sections.

4.1 Characterization and Application Pure and Composite Nanofiber:

4.1.1 Scanning Electron Microscopic (SEM) Analysis:

In order to examine the surface morphology of the nanofibers prepared by electrospinning of the gel solution were subjected to scanning electron microscopic (SEM) analysis. The SEM analysis confirmed the formation of cylindrical nanofibers of varying diameters. Figures 4.1 to Figure4.7show the microphotographs of ceria nanofibers having varying copper loadings (0 to 60 mole % Cu) prior to calcination. Green ceria nanofibers had an average diameter of about 130 nm (Figure4.1), whereas the average diameters of the green nanofibers containing 10, 20, 30, 40, 50 and 60 mol. % Cu were found to be 124, 117, 114, 108, 98 nm, and 109 nm, respectively. It is seen that after calcination, the average fiber diameter has reduced by about 20-30 % of the green fiber diameter. Tang et al (2012) has been prepared Pt/CeO_2 nanofibers by electrospinning method the average diameter of nanofibers ranged from 80 to 120 nm. Shan Xu and others reported an average diameter of green nanofiber as around 200nm (Xu et al; 2011). The reduction in diameter takes place due to the loss of PVP and other organic compounds during calcination (Fox et al; 2008).

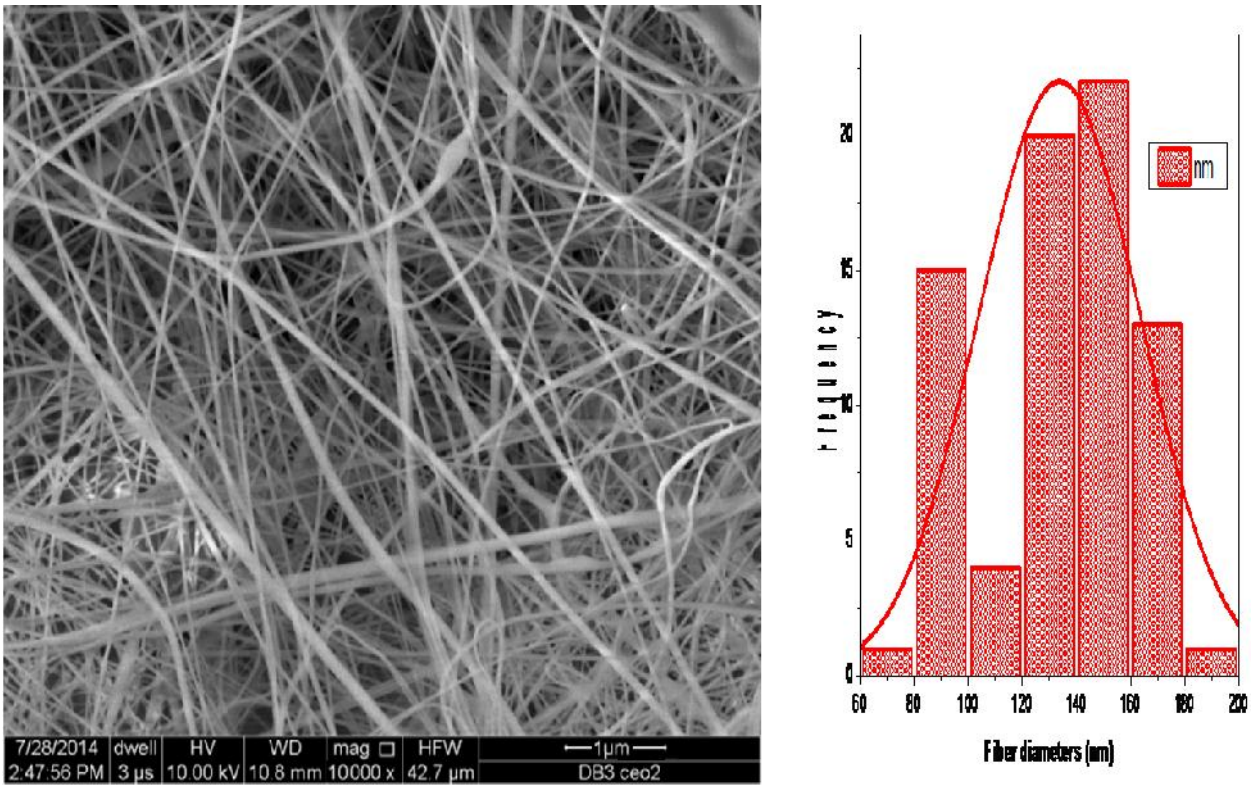

Figure 4.1 SEM spectra of pure ceria nanofiber with histogram.

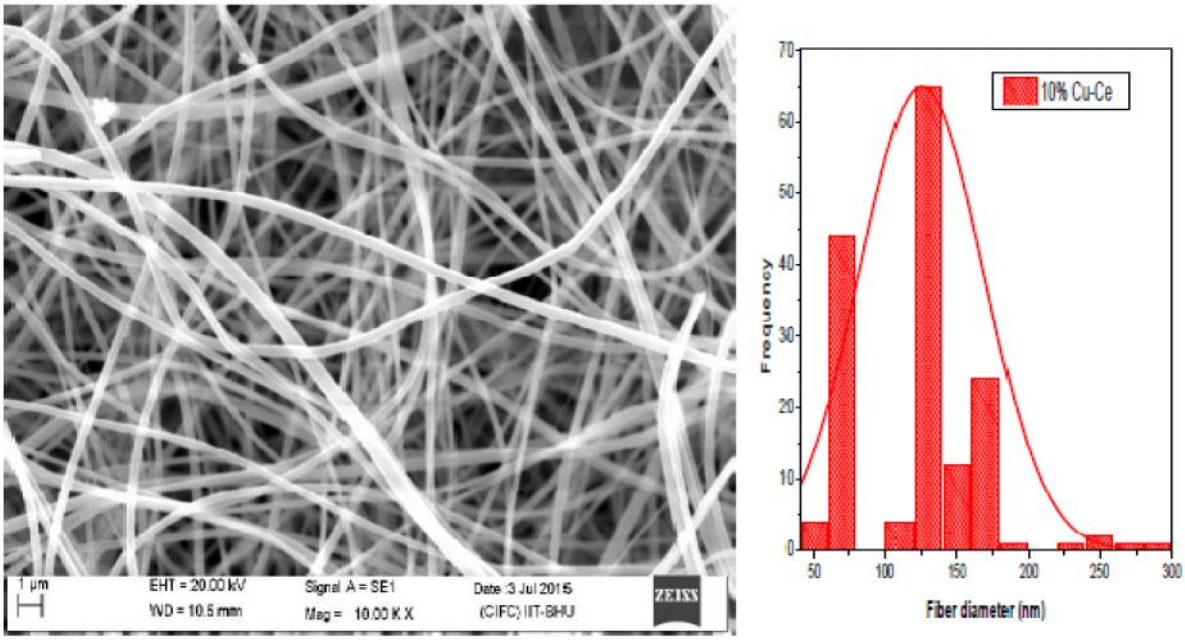

Figure 4.2 SEM spectra of 10 mol. % Cu loaded cerium nanofibers with histogram.

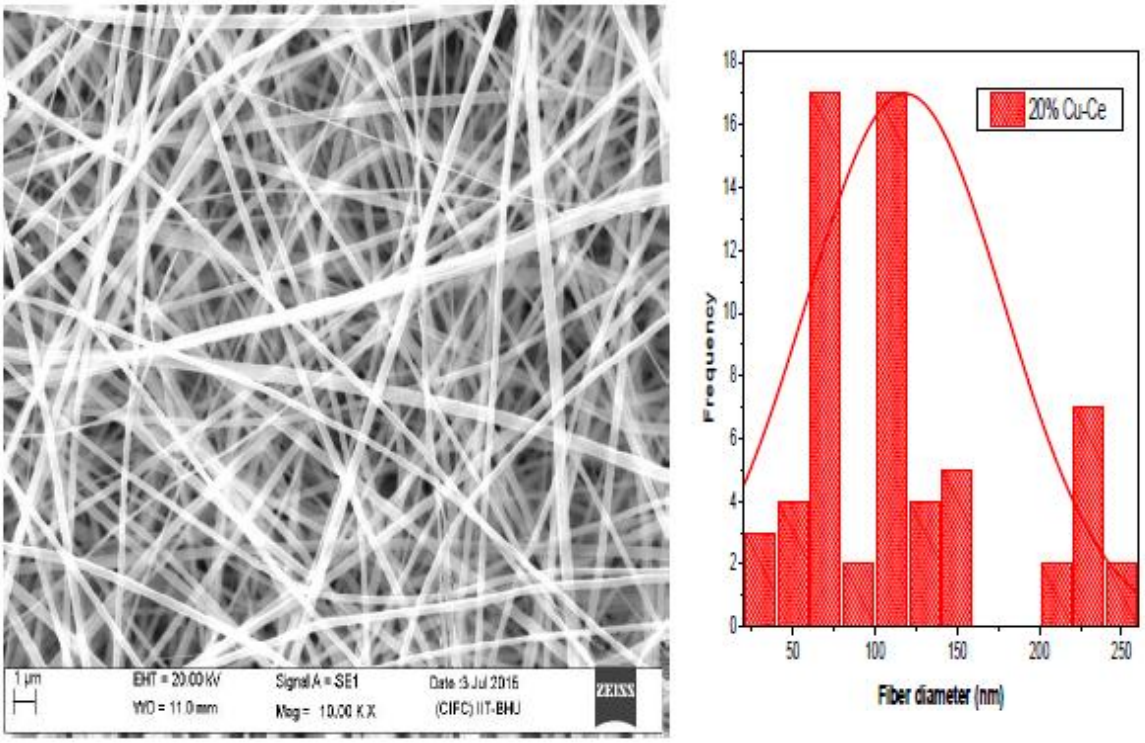

Figure 4.3 SEM spectra of 20 mol. % Cu loaded cerium nanofiber with histogram.

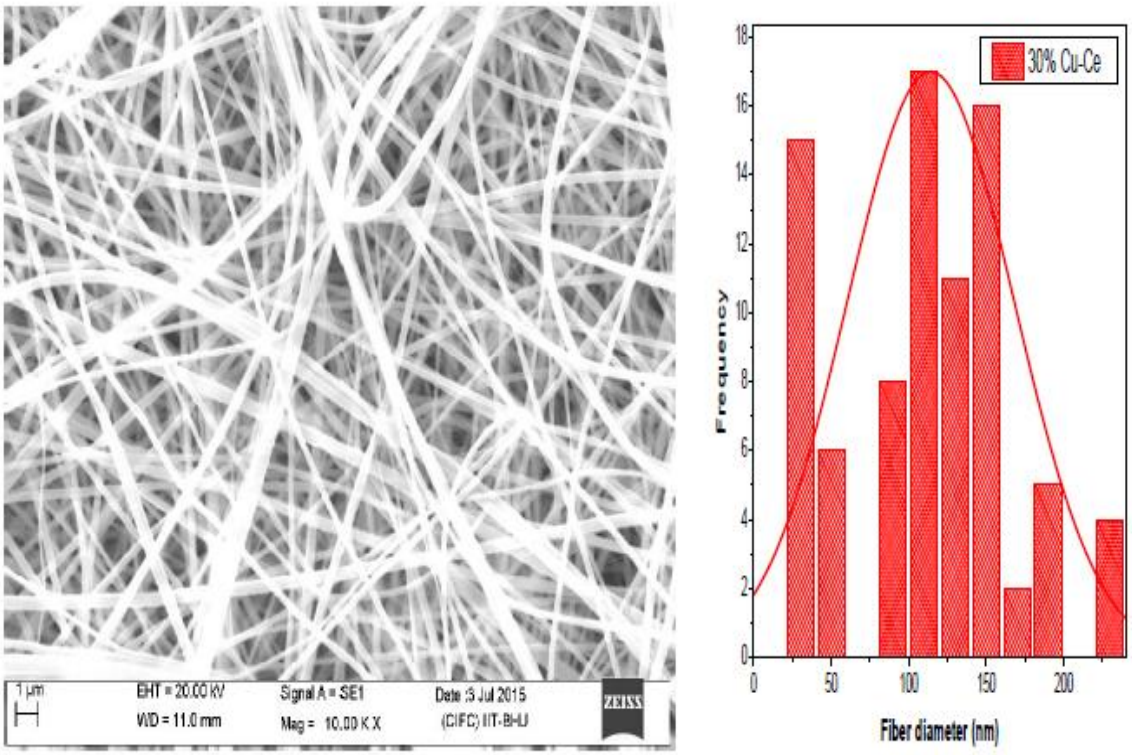

Figure 4.4 SEM spectra of 30 mol. % Cu loaded cerium nanofibers with histogram.

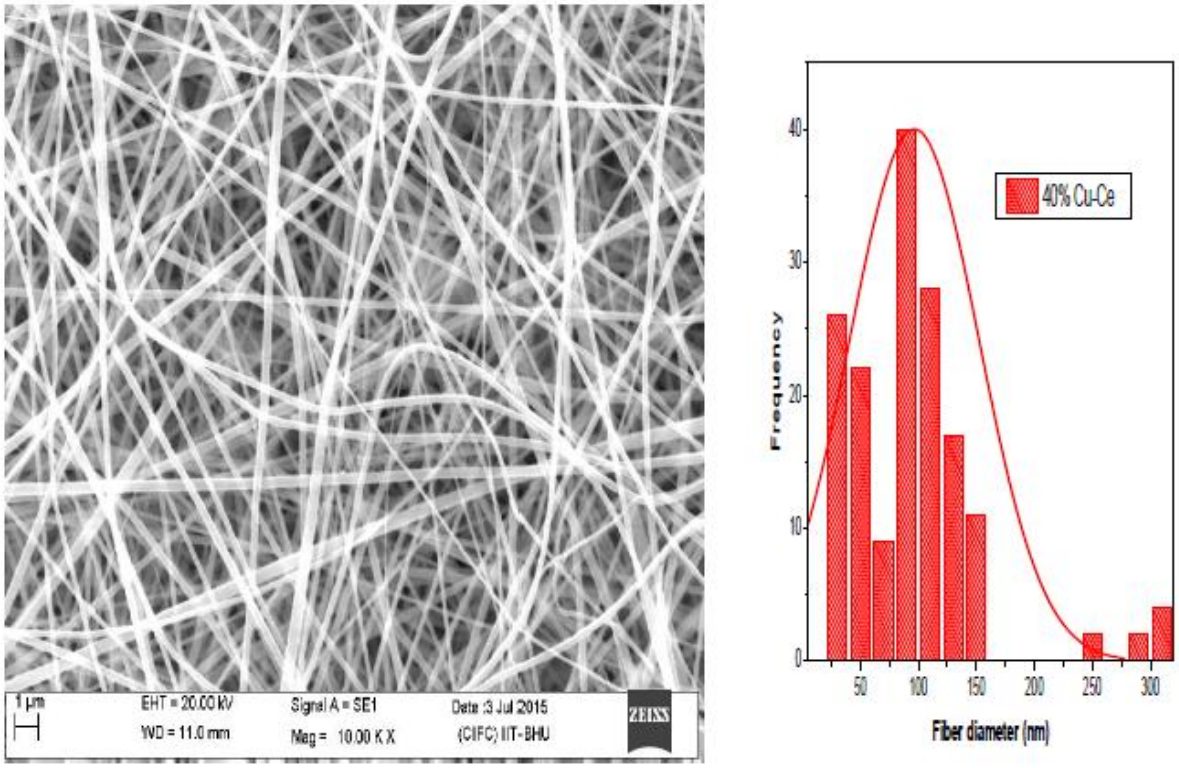

Figure 4.5 SEM spectra of 40 mol. % Cu loaded cerium nanofiber with histogram.

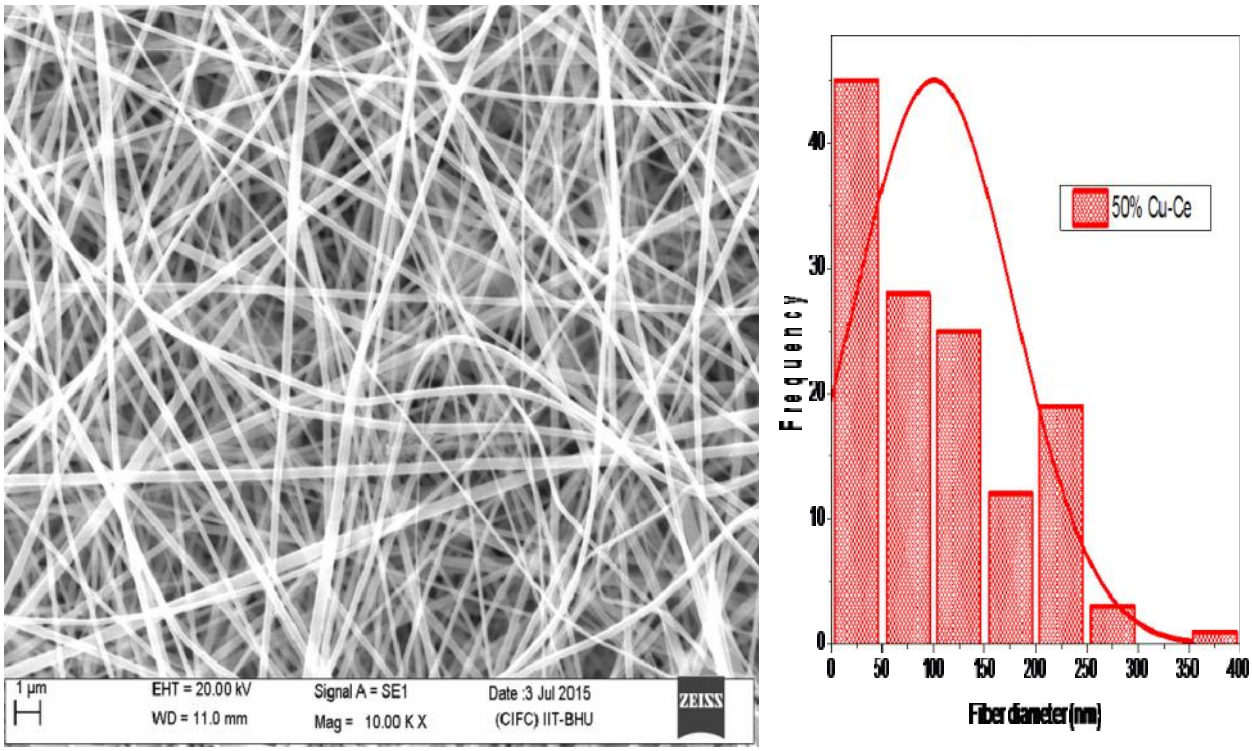

Figure 4.6 SEM spectra of 50 mol. % Cu loaded cerium nanofiber with histogram.

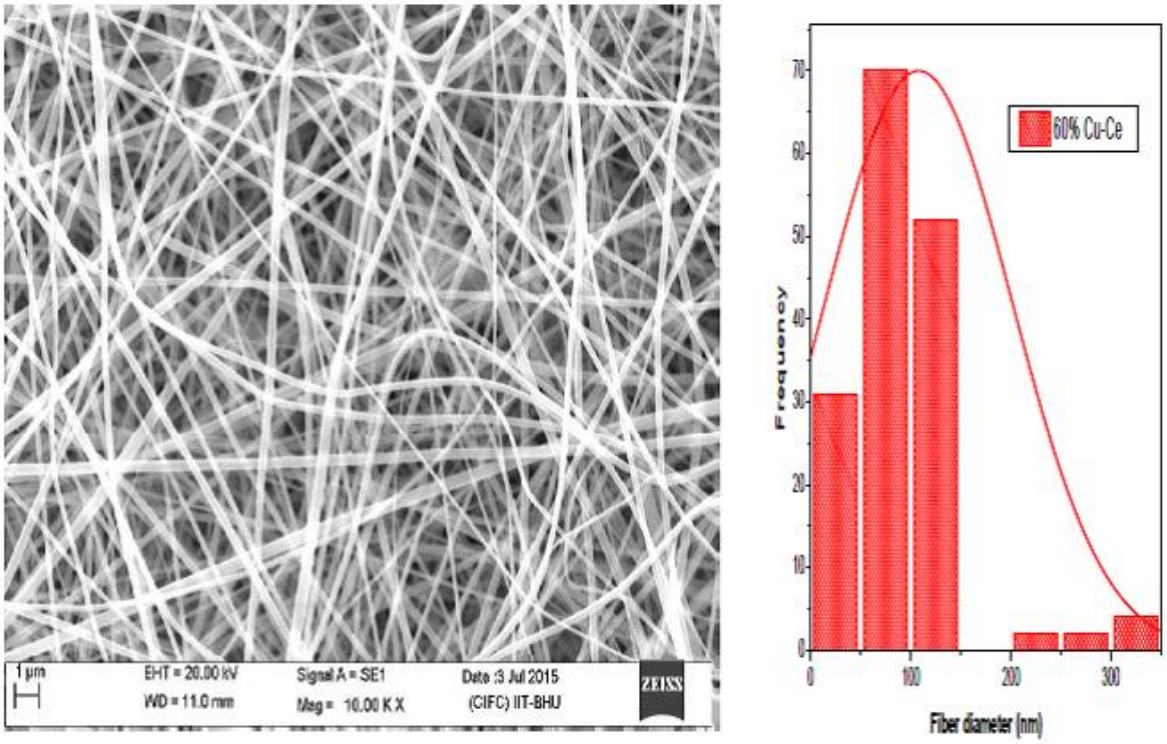

Figure 4.7 SEM spectra of 60 mol. % Cu loaded cerium nanofibers with histogram.

4.1.2 X-Ray Photoelectron Spectroscopy (XPS):

The Cu $2p^{3/2}$ spectrum shown in Figure 4.8 presents a challenge for interpretation because of the overlapping peaks of various Cu species in the binding energy (BE) range of 932 and 933 eV. Fox et al; (2008) discussed the presence of overlapping peaks for CuO and Cu^2O in this range and the dynamic behavior and mobility of Cu^2O, CuO and Cu^{x+} Ce due to oxidative /reductive conditions. As such, the Cu XPS must be considered along with the other characterization methods to fully elucidate the nature of the Cu ions in these catalysts (William et al; 2014). A possible explanation for the growth in relative strength is the reincorporation of surface CuO into the ceria lattice during oxidation at relatively higher temperature. The binding energy scale was calibrated by setting the main C 1s line of adventitious impurities at 284.7eV,

giving an uncertainty of ±0.2 eV in peak positions.This phenomenon strongly supports the results observed in C 1s XP spectra thus confirming that the decomposition of PVP occurred at 773 K.

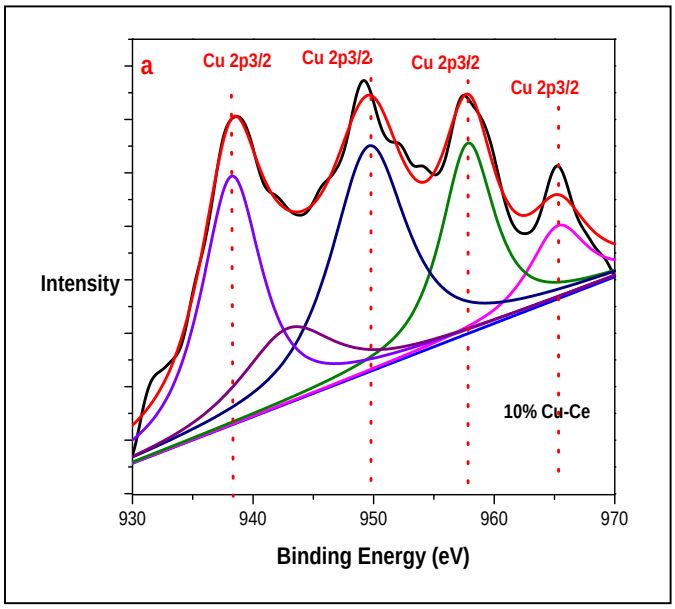

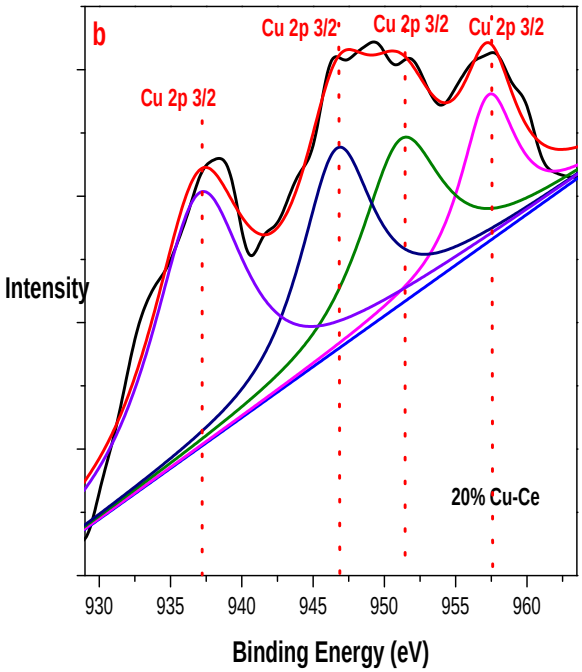

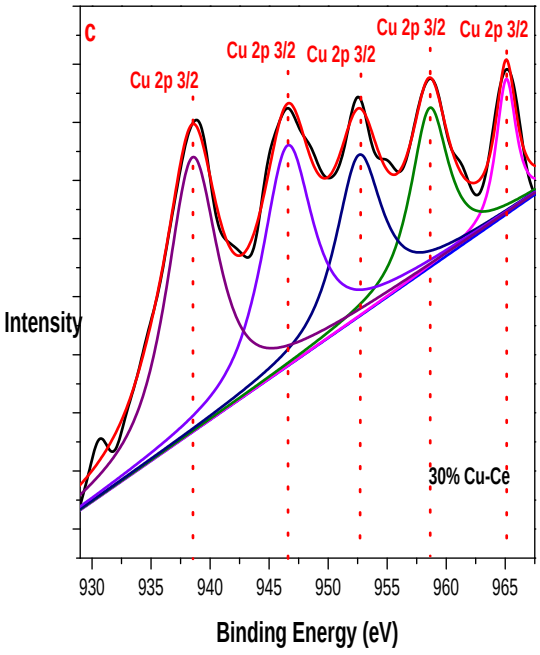

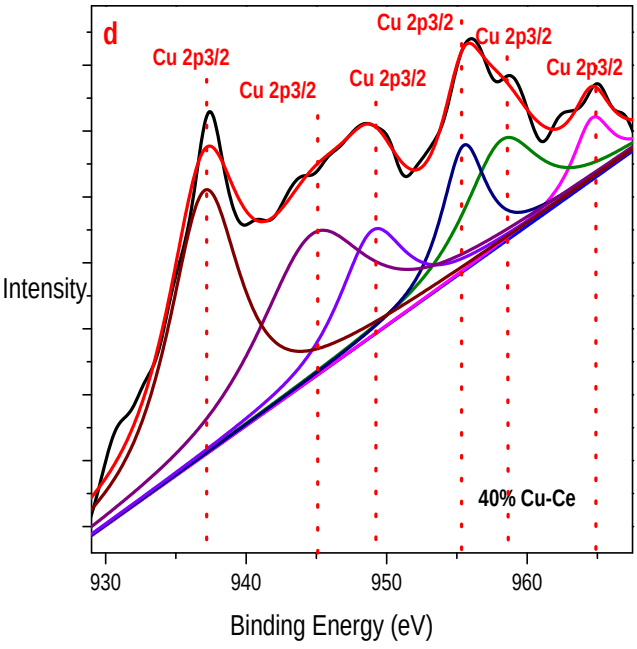

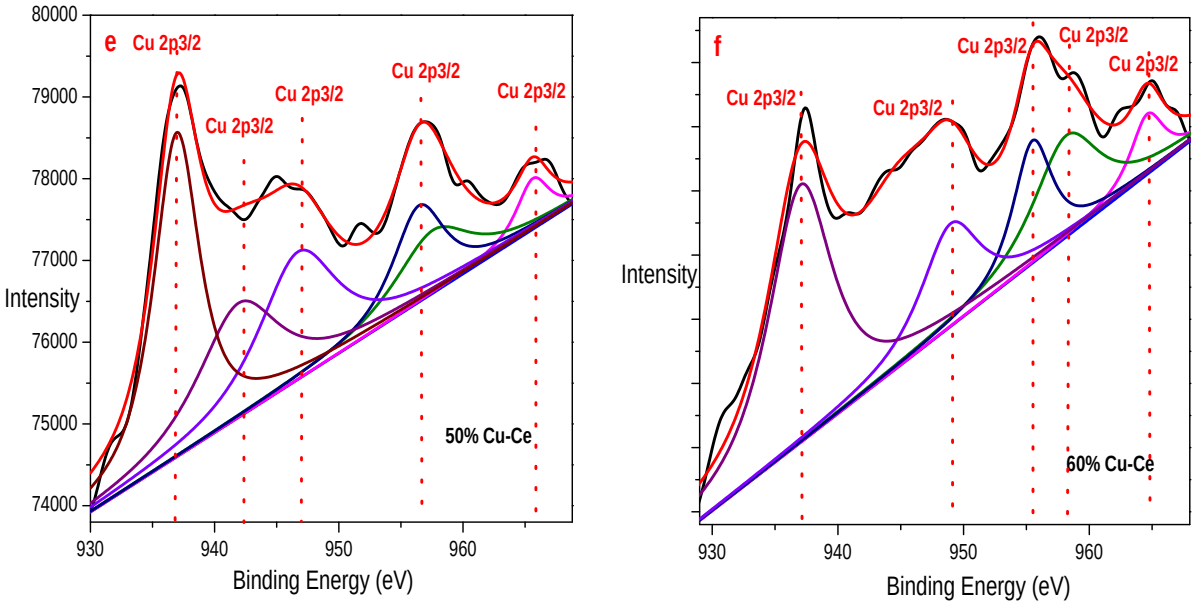

Figure 4.8 XPS spectra of Cu $2p^{3/2}$ in Cu/CeO_2nanofibers: (a) 10 mol. % Cu , (b) 20 mol. % Cu, (c) 30 mol. % Cu, (d) 40 mol. % Cu and (e) 50 mol. % Cu and (f) 60 mol. % Cu, loading respectively.

From Figure 4.9 it is seen that for O1s in the BE range of 529 and 530 eV. The interpretation of these spectra is also difficult due to overlapping peaks of various Ce and O species. The high resolution O 1s spectra of Ce oxide nanofibers are deconvoluted into two peaks: (i) oxygen species on the surface region (Hwang et al; 2011) and (ii) oxygen moieties bound with Ce^{3+} and Ce^{4+}. In calcinations of cerium nanofibers at 500ºC, the amount of oxygen bound with Ce^{3+} and Ce^{4+} increased and that of the surface oxygen decreased. Because the calcination causes the removal of surface oxygen, it is reasonable that the ratio of surface oxygen decreases. Therefore it is highly possible that calcination of Ce oxide nanofiber at high temperatures led to oxidation of Ce^{3+} to Ce^{4+}.

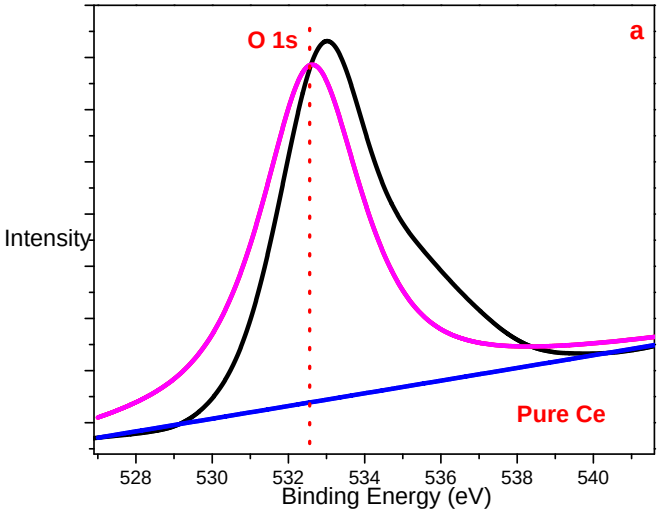
O 1s
a
Intensity
Pure Ce
528
530
532
534
536
538
540
Binding Energy (eV)

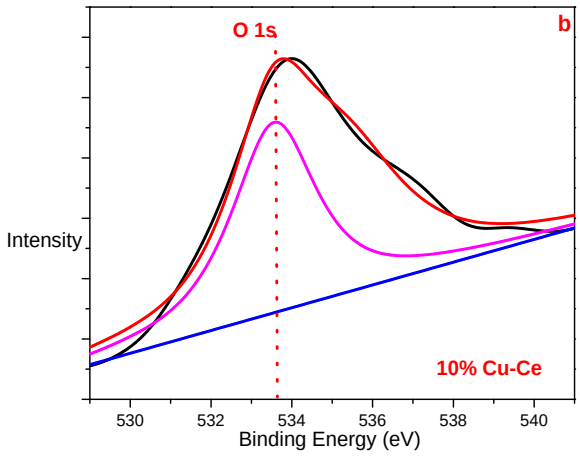
O 1s
b
Intensity
10% Cu-Ce
530
532
534
536
538
540
Binding Energy (eV)

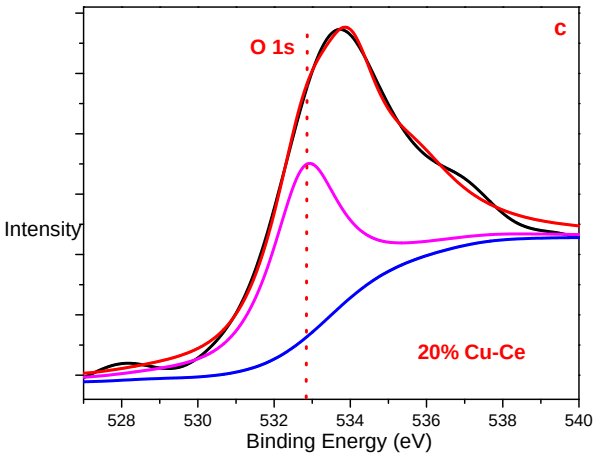
O 1s
c
Intensity
20% Cu-Ce
528
530
532
534
536
538
540
Binding Energy (eV)

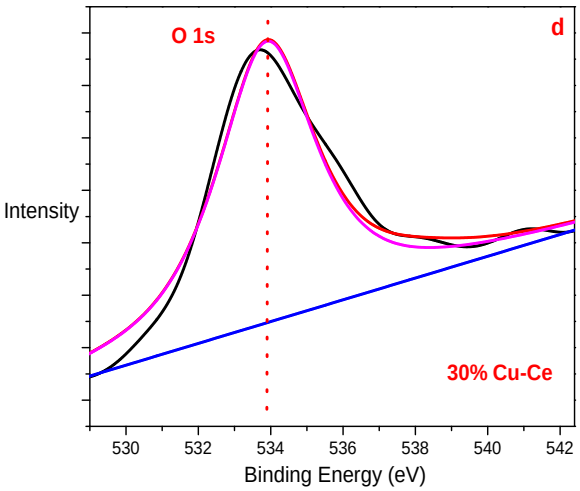
O 1s
d
Intensity
30% Cu-Ce
530
532
534
536
538
540
542
Binding Energy (eV)

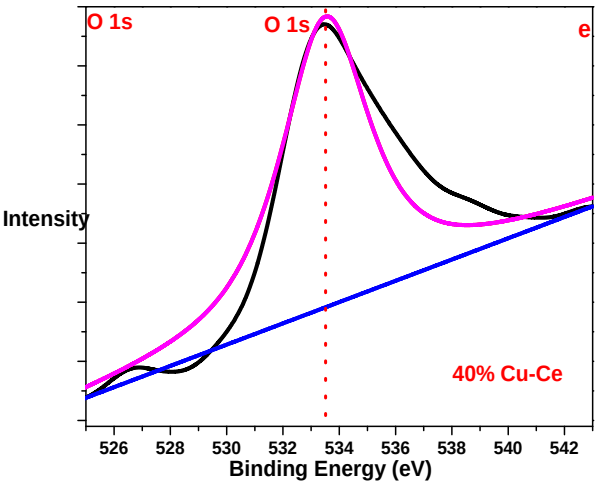
O 1s
O 1s
e
Intensity
40% Cu-Ce
526
528
530
532
534
536
538
540
542
Binding Energy (eV)

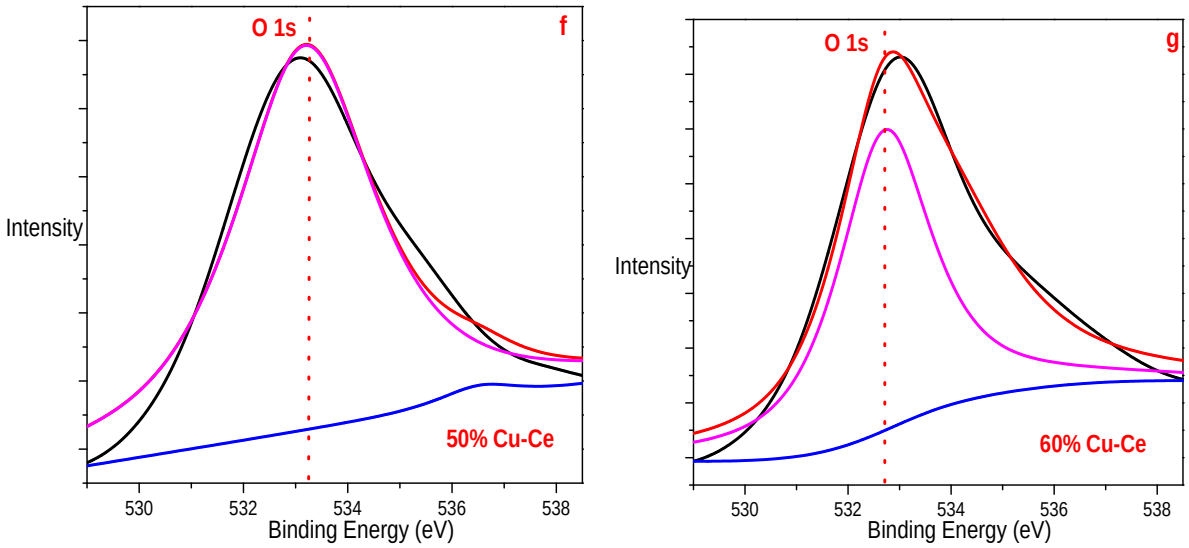

Figure 4.9 XPS spectra of O 1s in Cu/CeO_2 nanofiber: ceria (a), 10 mol. % Cu (b), 20 mol. % Cu (c), 30 mol. % Cu (d), 40 mol. % Cu (e) and 50 mol. % Cu (f) and 60 mol. % Cu (g), loading respectively.

Figure 4.10 shows the spectrum for $Ce3d^{5/2}$ in the binding energy (BE) range of 880 and 882 eV. The transition metal oxides, Ce oxide is one of the metal oxides which has various final states due to hybridization of Ce 4f and O 1s valence orbital's (Hwang et al; 2011). Cerium has two characteristic oxidation states (+3 and +4). The cerium 3d core level spectra are deconvoluted to 3 doublet peaks for Ce^{3+} and Ce^{4+} each. The initial state of Ce^{3+} is $3d^{10}4f^{1}$ and that of Ce^{4+} is $3d^{10}4f^{0}$. Three final states are assigned for Ce^{3+} and Ce^{4+}species each. In this study, u and v notations are used for the assignment of cerium 3d corresponding to $3d^{3/2}$ and $3d^{5/2}$, respectively.

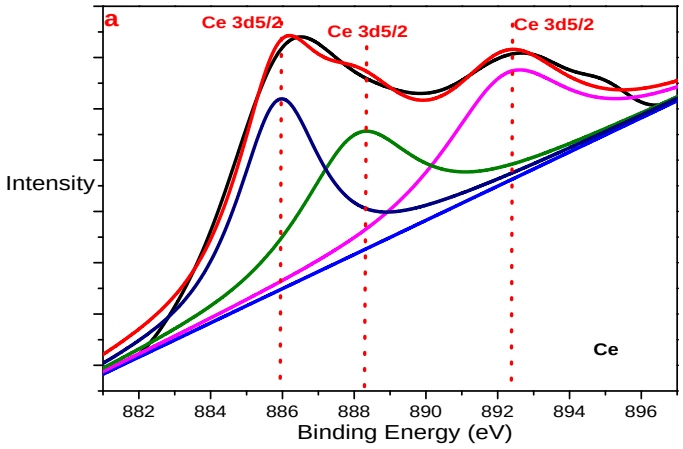
a
Ce 3d5/2
Ce 3d5/2
Ce 3d5/2
Intensity
Ce
882
884
886
888
890
892
894
896
Binding Energy (eV)

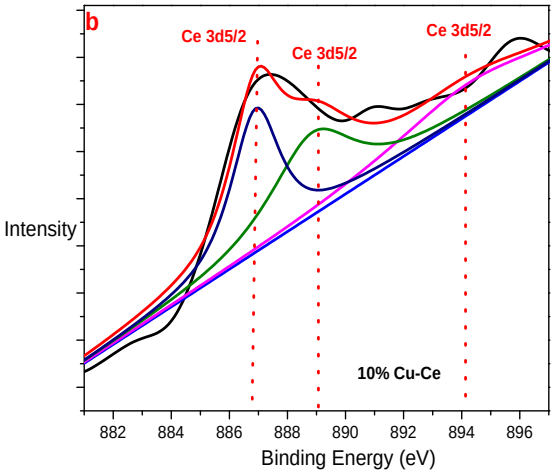
b
Ce 3d5/2
Ce 3d5/2
Ce 3d5/2
Intensity
10% Cu-Ce
882
884
886
888
890
892
894
896
Binding Energy (eV)

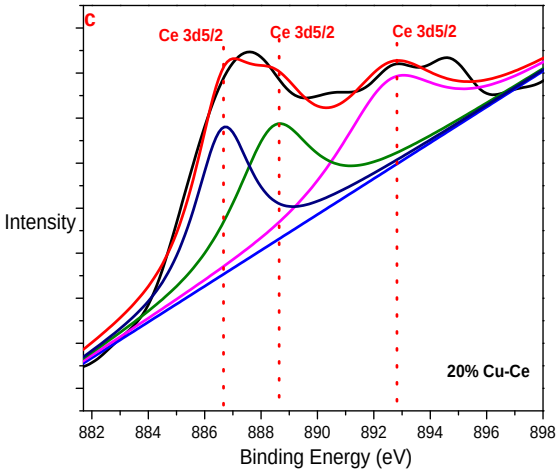
c
Ce 3d5/2
Ce 3d5/2
Ce 3d5/2
Intensity
20% Cu-Ce
882
884
886
888
890
892
894
896
898
Binding Energy (eV)

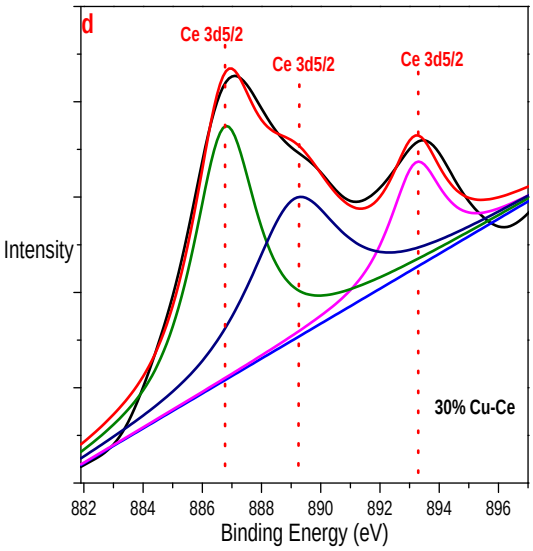
d
Ce 3d5/2
Ce 3d5/2
Ce 3d5/2
Intensity
30% Cu-Ce
882
884
886
888
890
892
894
896
Binding Energy (eV)

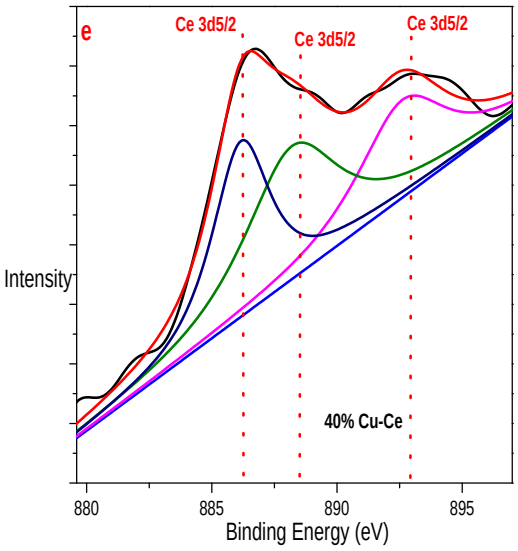
e
Ce 3d5/2
Ce 3d5/2
Ce 3d5/2
Intensity
40% Cu-Ce
880
885
890
895
Binding Energy (eV)

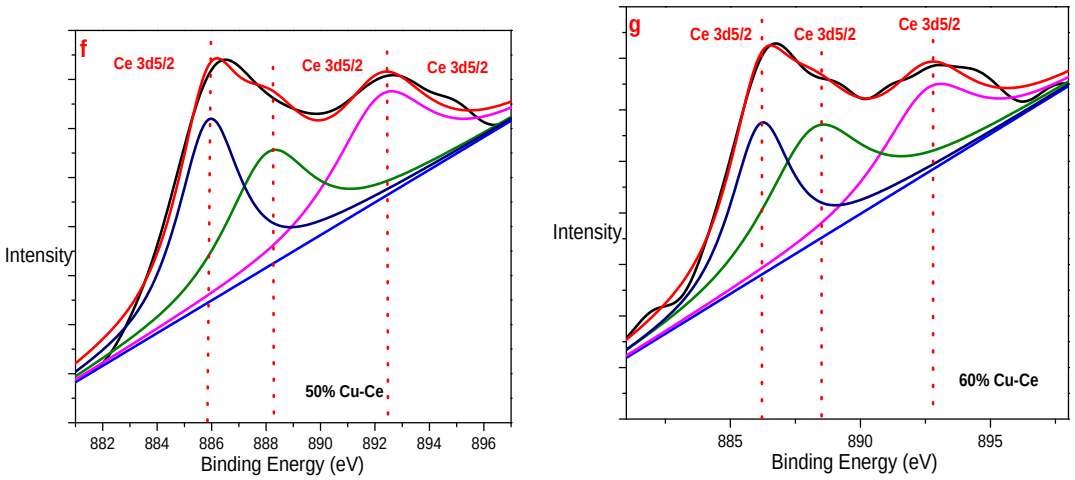

Figure 4.10 XPS spectra of Ce $3d^{5/2}$ in Cu/CeO_2 nanofibers: ceria (a), 10 mol. % Cu (b), 20 mol. % Cu (c), 30 mol. % Cu (d), 40 mol. % Cu (e), 50 mol. % Cu (f) and 60 mol. % Cu (g), loading respectively.

Table 4.1 lists the binding energy of different elements in the pure CeO_2 and CuO/CeO_2 composite. We need to find out the interaction among these metals. However,from the XPS data, it can be inferred that there was not any strong or weak interaction effect among these metals.

Table 4.1: Binding energy of the Cu $2p^{3/2}$, Ce $3d^{5/2}$ and O 1s levels in the catalyst.

Catalyst	**Cu $2p^{3/2}$ (B.E. in eV)**	**Ce $3d^{5/2}$ (B.E. in eV)**	**O 1s (B.E. in eV)**
CeO_2	-	886.8	928.0
10% Cu/CeO_2	933.8	886.5	932.00
20% Cu/CeO_2	934.8	886.4	932.02
30% Cu/CeO_2	935.2	886.3	932.25
40% Cu/CeO_2	935.4	886.3	932.40
50% Cu/CeO_2	935.8	885.5	932.50
60% Cu/CeO_2	934.9	885.3	932.40

4.1.3 Energy Dispersive X-Ray Spectroscopy (EDX):

In order to confirm the elements present in the synthesised nanofibers, the sample of the nanofibers before and after calcination was subjected to Electron dispersive X-ray spectroscopic (EDX) analysis. The analysis confirms copper loading of cerium oxide and also confirms the removal of organic compounds from the sample. The EDX finger-print exhibiting atomic compositions of the synthesized nanofibers are shown in Figures. 4.11 to Figure 4.17. These figures give the overall atomic composition of nanofibers of CeO_2 and Cu loaded ceria. From Figure 4.12 it is seen that atomic composition of Cu and Ce for 10 mol% Cu loaded ceria is 0.24% Cu and 1.63% Ce, which translates into a copper-cerium (Cu/[Cu + Ce]) mole fraction ratio of roughly 0.128 (~ 0.1). Similarly the (Cu/[Cu + Ce]) mole fraction ratio for 20, 30, 40, 50 and 60 mol% Cu loaded on cerium are (0.2) (Figure 4.13), (0.3) (Figure 4.14), (0.4) (Figure 4.15), (0.5) (Figure 4.16) and (0.6) (Figure 4.17), respectively. These results confirm the uniform distribution of Cu in the casting solutions. The EDX finger print reveals that the rough surfaces consist of a large amount of CuO while the smooth Surfaces are rich in CeO_2. For nanofibers catalysts, the preparation methods have less effect on the Cu/Ce ratio (Zhijian et al; 2015). These Cu-rich surfaces could be assigned to the bulk like CuO nanofibers. Since Cu is lighter than Ce, smaller CuO clusters that are interacting closely with CeO_2 could not be detected by SEM (Bickford et al; 2005).

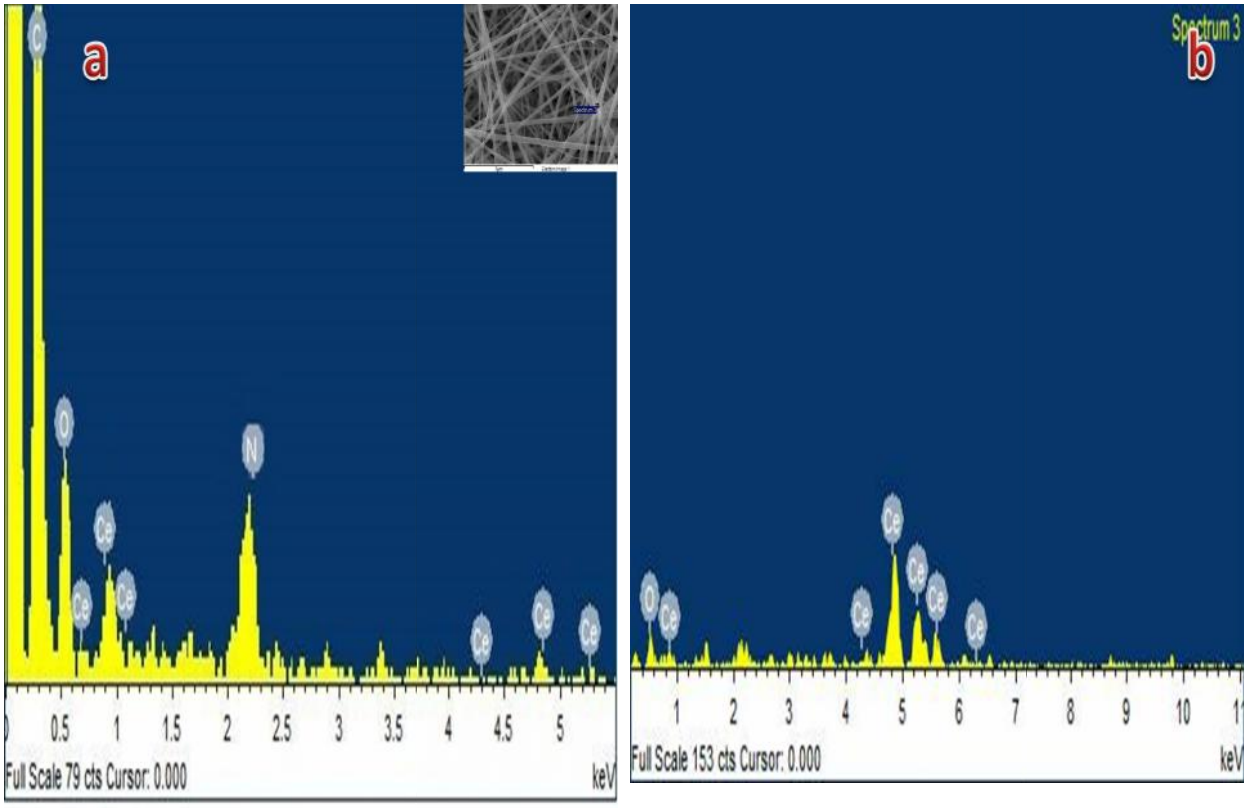

Figure 4.11 EDX spectra of pure ceria **a)** before and **b)** after calcinations of nanofiber

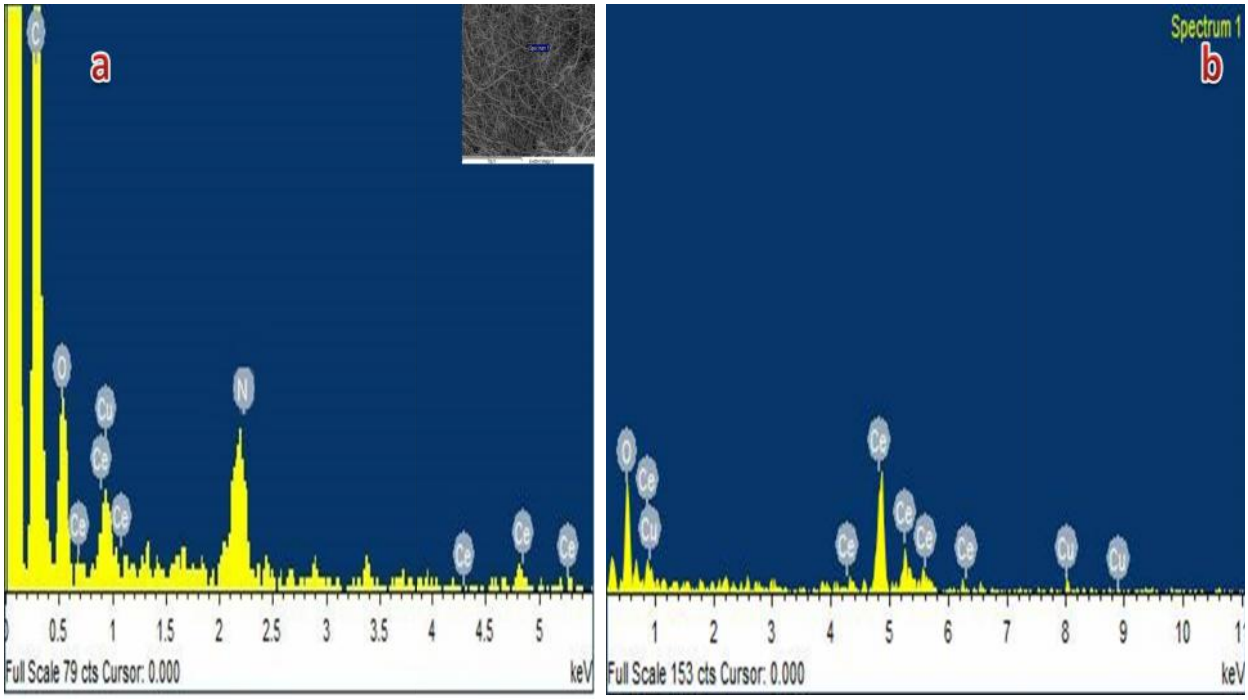

Figure 4.12 EDX spectra of 10 mol. % Cu loading on cerium **a)** before and **b)** after calcinations of nanofiber.

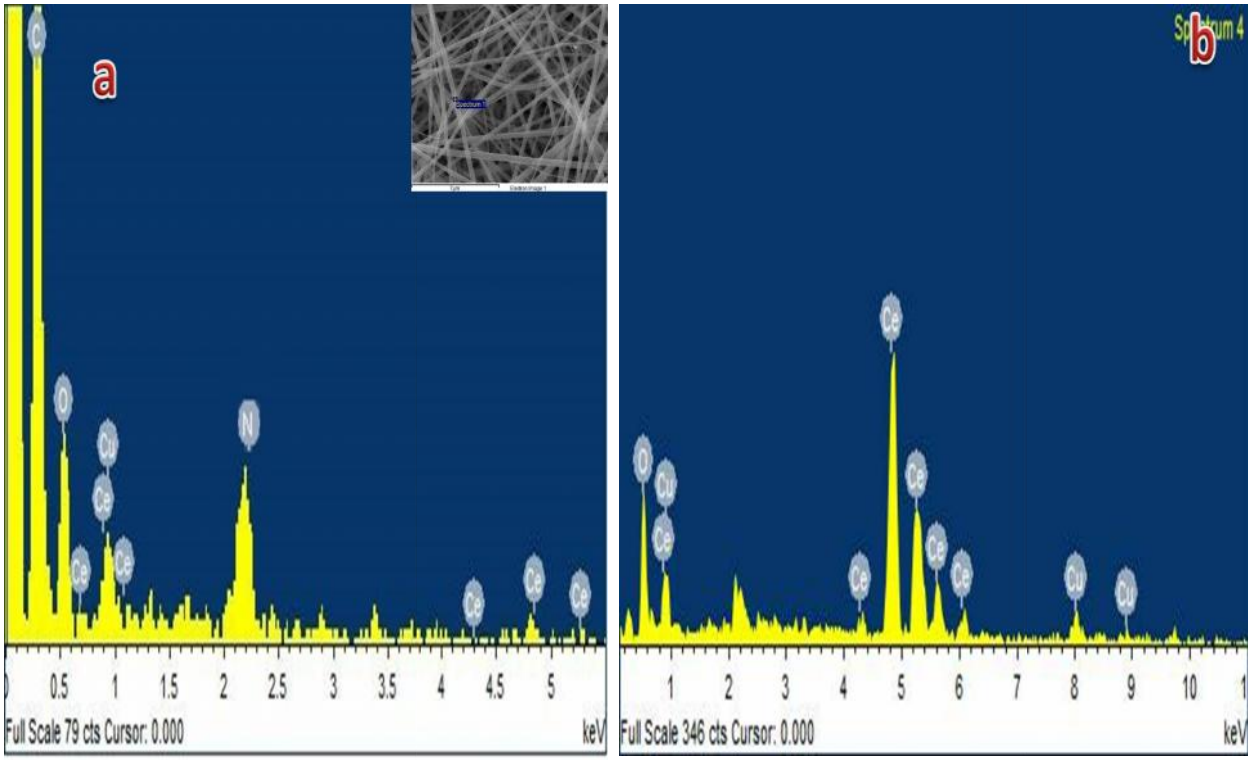

Figure 4.13 EDX spectra of 20 mol. % Cu loading on cerium **a)** before and **b)** after calcinations of nanofiber.

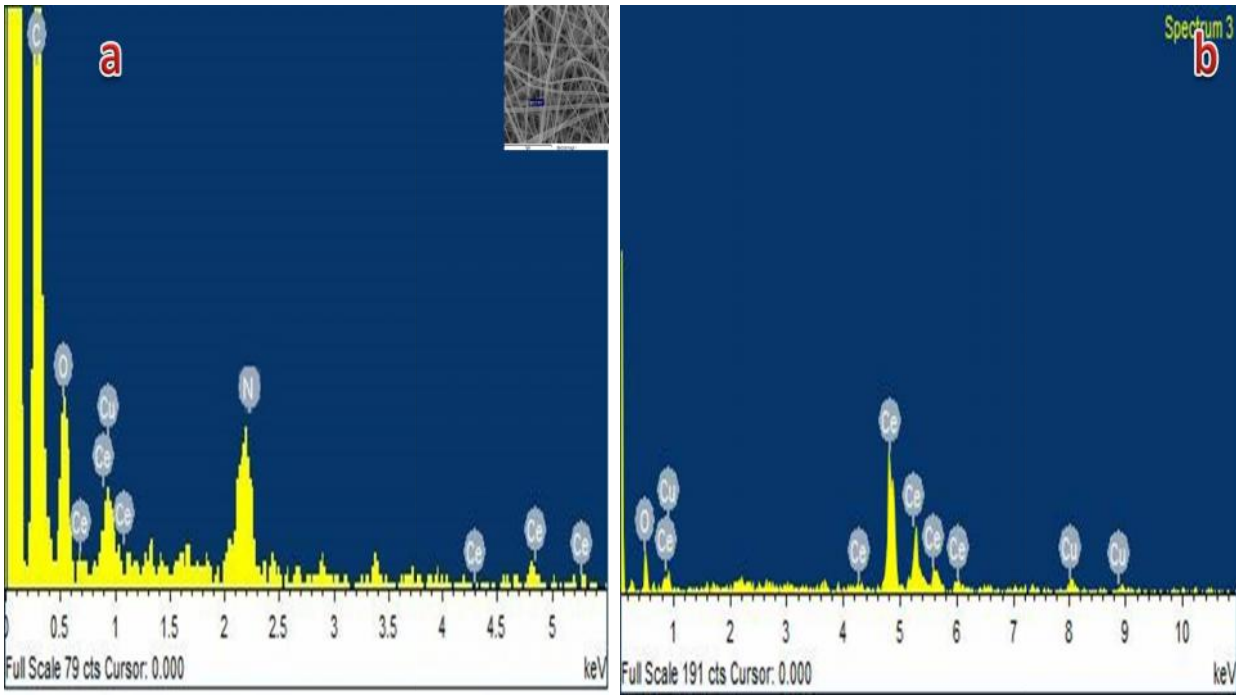

Figure 4.14 EDX spectra of 30mol. % Cu loading on cerium a) before and b) after calcinations of nanofiber.

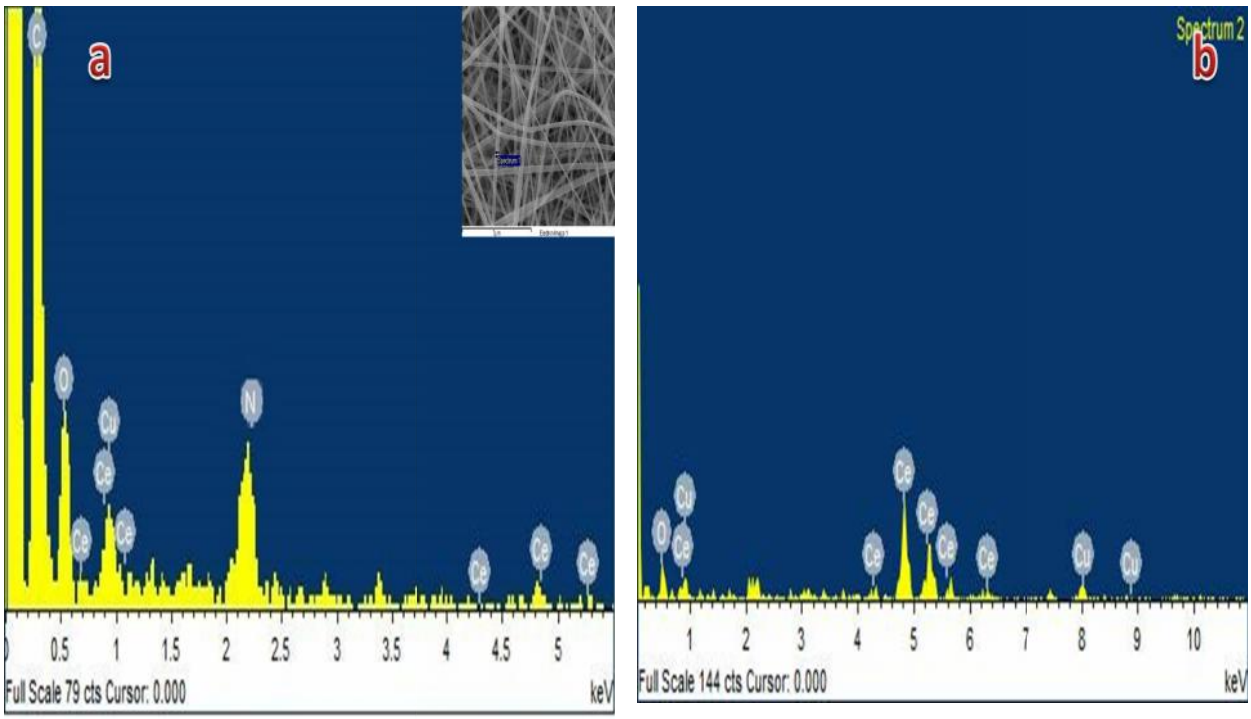

Figure 4.15 EDX spectra of 40mol. % Cu loading on cerium **a)** before and **b)** after calcinations of nanofiber.

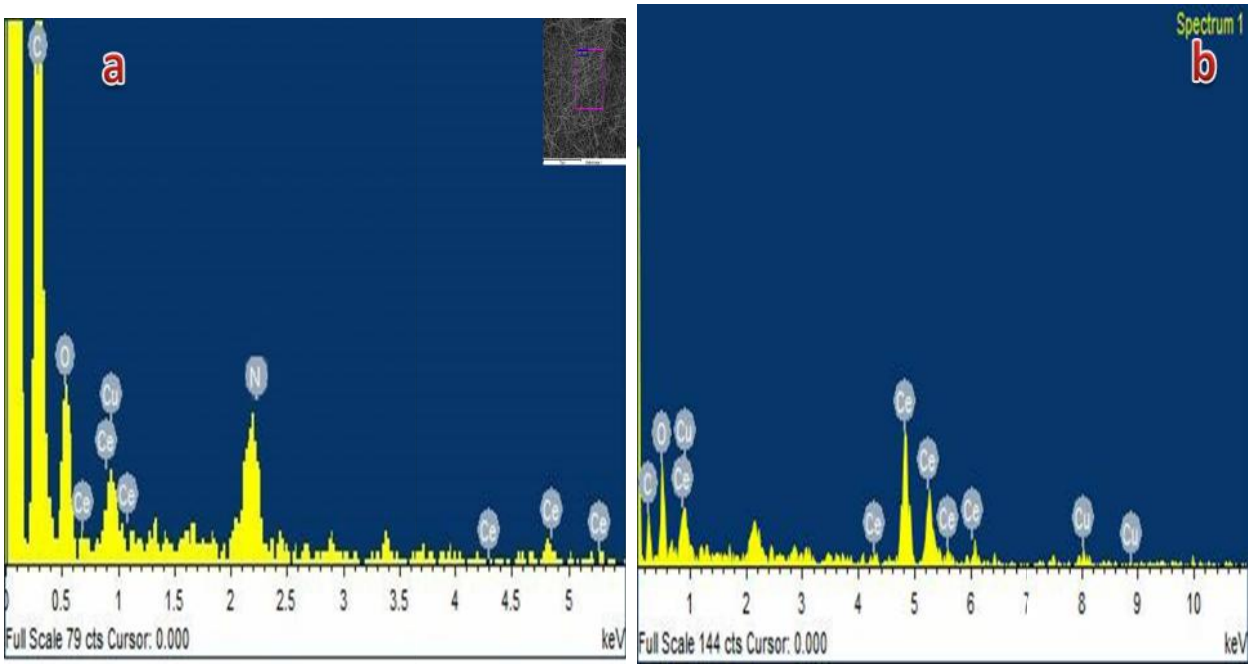

Figure 4.16 EDX spectra of 50mol. % Cu loading on cerium a) before and b) after calcinations of nanofiber.

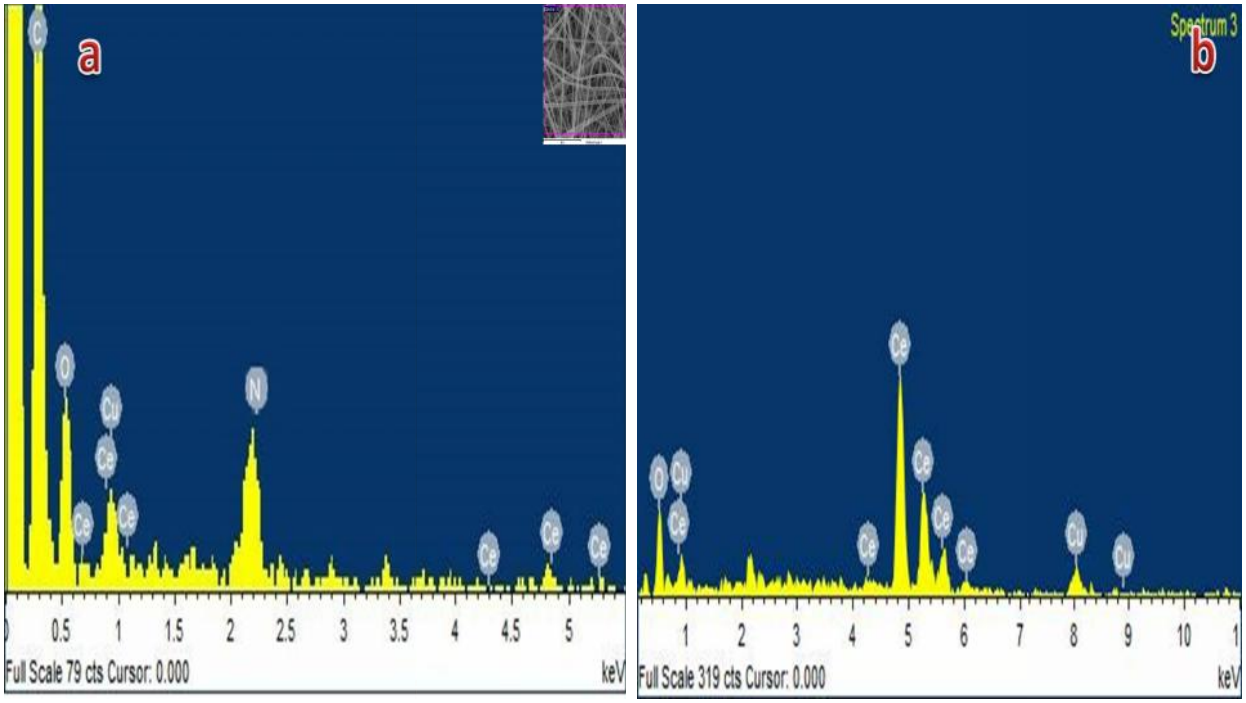

Figure 4.17 EDX spectra of 60 mol. % Cu loading on cerium **a)** before and **b)** after calcinations of nanofiber.

4.1.4 Fourier Transforms Infrared (FTIR) Analysis:

The FTIR spectra of CeO_2 and CuO/CeO_2 nanofibers are given in Figure 4.18. The broad band's present between 3700 to 3000 cm^{-1} are due to the stretching vibration of hydroxyl (OH) group of chemisorbed water. The disappearance of peaks (900-1630 cm^{-1}) after calcination of CeO_2 and CuO/CeO_2 nanofibers at 500°C indicates removal of most of the organic materials present in the sample. The significant enhancement in the absorption band at 500-1060 cm^{-1} represents formation of CeO_2 nanofiber. Some authors (Liu et al; 2008; Girija et al; 2011) have reported that these stretches may be assigned to the O–H from the residual water, the C-C and C-H from the residual polymer, and stretches below 1200 cm^{-1} to the Ce-O bonds. The spectra show some bands around 3440, 1630 and 1385 cm^{-1} and several stretches below 1200 cm^{-1}, that are more clearly evident in the green samples containing copper acetate and cerium nitrate.

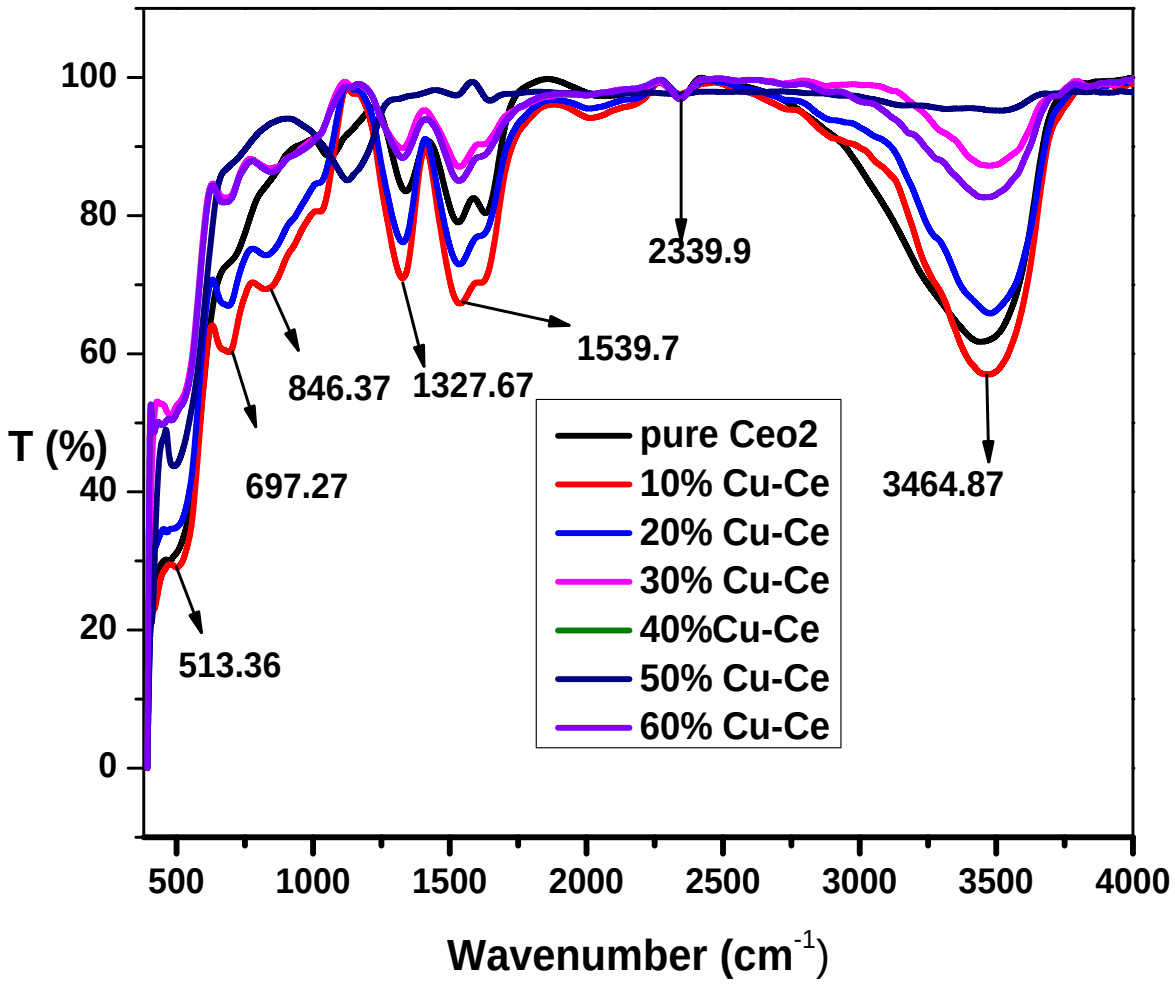

Figure 4.18FTIR spectra of Ceria and composite copper-ceria nanofibers

4.1.5 Thermo-gravimetric Analysis (TGA):

The results of TGA of the PVP/cerium nitrate composite/ copper acetate fibers are shown in Figure 4.19, two major mass loss peaks were observed. The first mass loss peak up to 240°C, is due to the removal of water of crystallization in (Eq. 4.1) and other organic compound removals. The second mass loss is observed between 400 and 450ºC, and is due to the decomposition of anhydrous $Ce(NO_3)_3$ to CeO_2 (Eq. 4.2), $Cu(CH_3COO)_2$ to CuO (Eq. 4.4) and oxides of nitrogen (Singh et al; 2010). which indicate that most of the organics which belonged

to PVP, NO_3 groups of cerium nitrate, and other volatiles were removed at temperature above 450°C and when 10 to 60% copper was loaded in cerium the stability of fiber increased above 950°C but in case of pure green nanofiber stabilized at 850°C.

$$Ce(NO_3)3.6H_2O = Ce(NO_3)3 + 6H_2O \quad (4.1)$$

$$Ce(NO_3)3 + O_2 = CeO_2 + Oxides\ of\ nitrogen \quad \Delta H \sim -\frac{121kj}{mol} \quad (4.2)$$

$$Cu(CH_3COO)2.H_2O + O_2 = Cu(CH_3COO)_2 + 6H_2O \quad (4.3)$$

$$Cu(CH_3COO)2 + 4O_2 = CuO + 4CO_2 + 3H_2O \quad (4.4)$$

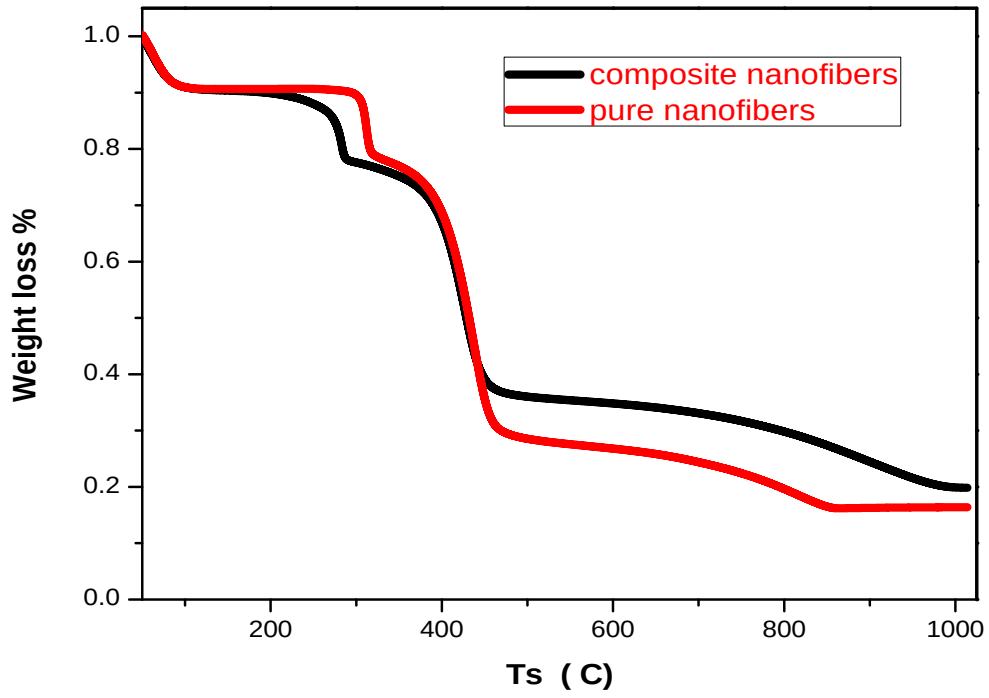

Figure 4.19 TGAanalysisof green Ceria and composite copper-ceria nanofibers

4.1.6 X-Ray Diffraction Analysis:

The diffraction patterns have been indexed by comparison with the JCPDS files. The XRD patterns of the CeO_2 and CuO/CeO_2 nanofibers with different copper loadings (0-60 mol. % Cu) are depicted in Figure4.20. The graphs exhibit characteristic peaks of a fluorite-like cubic

phase. No peaks are observed for nanofibers at room temperature regardless of the concentration of cerium nitrate. This indicates that nanofibers obtained at room temperature by the electrospinning technique are amorphous (Qizheng et al; 2008). After calcinations, the diffraction peaks for cubic CeO_2 appeared as identified by JCPDS database. The most intense reflection of CeO_2 is due to cubic fluorite structure with h, k, l value (1, 1, 1), JCPDS (340394) and monoclinic CuO structure with h, k, l value (2, 0, 2), JCPDS (801917) at 2θ values of 28.83° and 46.78^{0} respectively. Others are due to CeO_2 having structure with h, k, l values (2, 0, 0) at 2θ values of 34.83°, CeO_2 h, k, l values (2, 2, 0), at 2θ values of 58.83° , CeO_2 having structure h, k, l values (2, 2, 0), at 2θ values of $68.83^{\circ}$and CuO have structure, h, k, l value (2, 0, 2), at 2θ values of 39.03°, CuO have monoclinic structure with h, k, l values (2, 2, 0), at 2θ values of 69.83° . The average crystallite size of CeO_2 (15 nm) and CuO/CeO_2 (9-12 nm) were calculated by Scherer formula. Rajendran et al; (2013) also obtained ceria with crystalline size 12-16 nm. For ceria-CuO catalyst it has been reported that Cu impregnation influences the ceria lattice parameter marginally (Raitano et al; 2012). Competing effects are at play when doping the fluorite like lattice of ceria with the divalent Cu^{2+} cations. The smaller ionic radii of both Cu and Cu^{2+} suggest that doping will lower the lattice parameter, but increased vacancies and lattice distortion due to doping will increase the lattice parameter (Raitano et al; 2012).

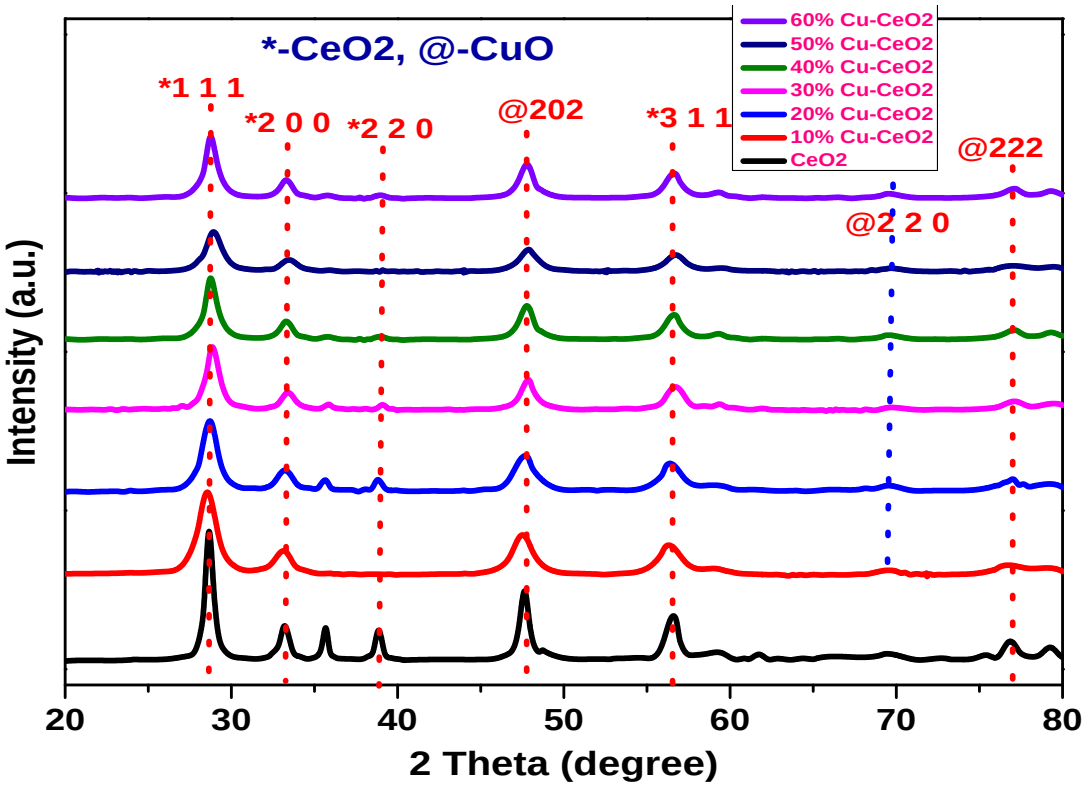

Figure 4.20XRD spectra of nanofiber calcined at 500°C for 3hrs.

4.1.7. Brunauer Emmett Teller (BET) Surface Area:

The physisorption has low degree of specificity and forces responsible for this phenomenon are similar to condensation of vapors and the deviations from ideal gas behavior. The molecule of fluid keeps its identity along the adsorption-desorption from ideal gas process. It is always exothermic and the low interactions involved are of Van der Waals type. At high pressures, they generally occur as a multilayer.

$$\frac{p}{n(p^o - p)} = \frac{1}{n_m C} + \frac{C-1}{n_m C} \times \frac{p}{p^0} \qquad (4.5)$$

Where n = specific amount of the gas adsorbed at the equilibrium pressure p,

n_m= monolayer capacity and p^o = saturation pressure. C = constant, assumed to be exponentially related to the adsorption energy.

The BET plot represents a straight line with slop of $(C-1)/n_m$ C and intercepts of on the Y axis equivalent to $1/n_mC$. The specific surface area, A_{BET} can be obtained from the BET monolayer capacity n_m by applying the following simple relation $A_{BET} = n_mLa$

Where L= Avogadro constant and A= average area occupied by each molecule in the complete monolayer. It presents important limitations and is applicable in a restricted p/p^o range (0.05 - 0.3). BET surface area of CuO/CeO_2nanofiber as prepared in ambient air and calcined at temperatures 500°C for 3hrs. The surface area of ceria nanofiber was 89 m^2/g and composite CuO/CeO_2nanofiber (10-60 mol% Cu) surface area was 98-129 m^2/g. It has been with increasing copper loading above 50 mol%, the BET area of the catalysts decreased. It is not necessary that copper loading on ceria decreases BET surface area due to pore blockage. It is because of the mutual interaction between CuO andCeO_2in $CuO-CeO_2$catalysts, which is translated to enhance the surface area (Gunawardana et al; 2009).

Table: 4.2 Comparative summary of surface area and crystalline size of catalyst

S. N.	Catalyst	BET surface area[a] (m^2/g)	Average Crystalline Size of Nanofibers[b] (nm)	Ref.
1	CeO_2	89	14.94	Present study
2	10-60% Cu/CeO_2	98-129	9-12	Present study
3	La doped CeO_2	91.7	15-18	Li et al. [2000]
4	CeO_2	215	14-19	Bickford et al. [2005]
5	nanosized CeO_2 and doped CeO_2	90-150	16-20	Fu et al. [2003]

Table 4.3 clearly shows that the surface area (Determined by N_2 adsorption-desorption measurement) increases with a decrease in the crystallite size and diameter of nanofiber catalysts

upto 0-50% copper loading. With further increase in copper loading, surface area decreases, whereas the crystalline size (calculated by X-ray line broadening method using Sherrer equation) and diameter (average nanofiber diameter measured by Image-J software) increase.

Table: 4.3 Surface area and Textural properties of all catalyst

S. N.	**Catalyst**	**BET surface area[a] (m^2/g)**	**Average Crystalline Size of Nanofibers[b] (nm)**	**Average diameter of Nanofibers[c] (nm)**
1	CeO_2	89	14.94	130
2	10% Cu/CeO_2	98	12.03	124
3	20% Cu/CeO_2	109	12.67	117
4	30% Cu/CeO_2	120	10.45	114
5	40% Cu/CeO_2	125	9.78	108
6	50% Cu/ CeO_2	129	8.90	98
7	60% Cu/CeO_2	124	10.03	109

[a]Determined by N_2 adsorption-desorption measurement.

[b]Calculated by X-ray line broadening method using Sherrer equation.

[c]Average nanofiber diameter evaluated by Image-J software.

4.1.8. Catalytic Activity of Cu-Ce Oxide Nanofibers for Water Gas Shift Reaction:

Figure 4.21 compares the results for various catalysts as a plot of CO conversion versus temperature. All the prepared catalysts were evaluated for their effectiveness in catalysing the water gas shift reaction in the temperature range of 25-400^oC. It can be clearly seen that the equimolar copper-ceria nanofiber (50% Cu) is the best catalyst giving maximum CO conversion

of 78% at 295^{0}C, whereas the pure ceria nanofiber gives the lowest CO conversion of 68% at the same temperature. The activities of various catalyst are in the order of 50% CuO/CeO_2 > 60% CuO/CeO_2 >40% CuO/CeO_2 > 30% CuO/CeO_2 > 20% CuO/CeO_2 > 10% CuO/ CeO_2> CeO_2, respectively. It is seen that, the CO conversion with 50% CuO/CeO_2 nanofiber catalyst was higher than that over the pure CeO_2 catalysts with the temperature range of 150-400°C. From this figure, it is observed that increasing the reaction temperature results in decreasing CO conversion hence the H_2 yield. This provides evidence that the WGS reaction is favorable at low temperature. Jeong et al; (2015) studied the effectiveness of Pt/CeO_2 nanocatalyst prepared with the optimized synthesis parameters and obtained highest CO conversion (82%). Tang et al; (2012) used Pt/CeO_2 nanofibers prepared by electrospinning method and obtained CO conversion of 98%, at 300^{0}C, whereas ceria nanofibers impregnated with Pt showed ~50% CO conversion. Tibiletti et al; (2005) investigated the activities for $Au/Ce/ZrO_4$ and obtained 50% conversion at 210 °C and the equilibrium conversion were only achieved at 450°C. Xing et al; (2012) investigated the catalytic activity of $La/CuO/CeO_2$ gave the highest CO conversion around 93.1% at 250°C. Elise et al; (2005) investigated the oxygen-assisted water gas shift reaction over a $Cu\text{-}Pd/CeO_2$ nanomaterial synthesized by urea gelation and obtained conversion close to 99% even under extremely high H_2 concentration. Li et al; (2008) used Au/Fe_2O_3 catalyst prepared by modified DP method and that showed a very high activity at low temperatures, with a CO conversion above 80% at 150^{0}C. Maciel et al; (2013) used Cu-Ce-Ti catalyst and reported CO conversion of 63% at 450^{0}C. The conversion of CO was only 45% and 11%, respectively using catalyst Cu-Ce and Cu-Ti (Maciel et al; 2013). Cu-based catalysts have proved to be excellent candidates for the low temperature WGS reaction due to their high activity and low cost. Ceria, with controlled morphology and ability to expose different crystal planes to the solid crystallite, exhibits interesting chemical and physical properties, which can be

closely linked to the catalytic activity of CuO/CeO_2 catalysts. On the basis of the above results, it can be found that the morphology of the CeO_2 support has a notable effect on the dispersed state of the deposited Cu species and the interaction between Cu and the support, and then goes a step further to greatly affect the catalytic activity of the nanofiber catalysts.

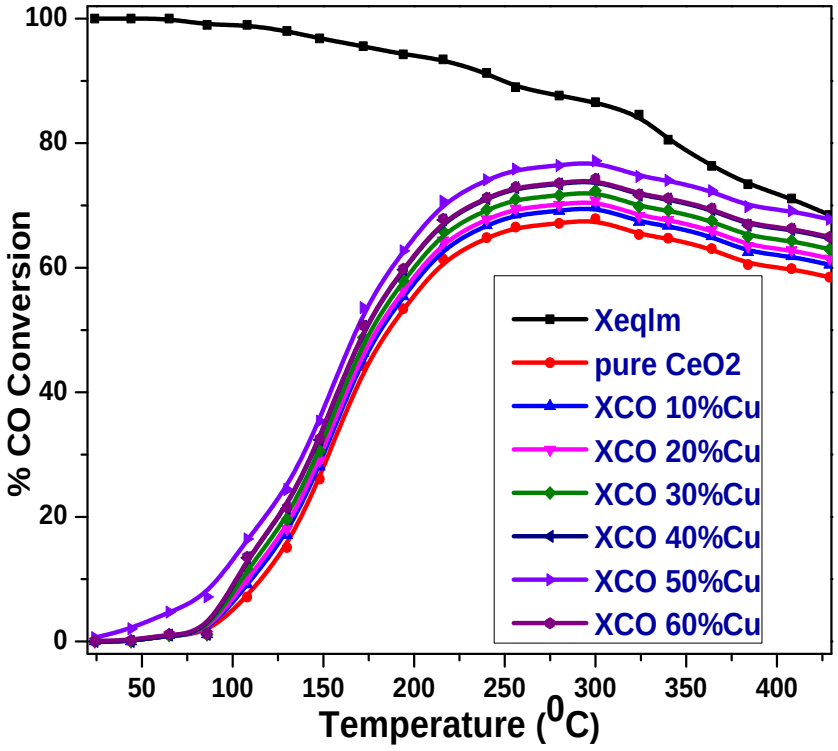

Figure 4.21comparative study copper-cerium oxides composite nanofiber catalyst during WGSR runs in 150-400^{o}C feed gas flow rate, 1.5 ml/min. CO, 58.50 N_2 ml/min and water vapors

Table 4.4 clearly shows that CeO_2 and CuO/CeO_2 composite nanofibers prepared by electrospinning method and used in the present study gave 78% CO conversion at the lowest temperature (295^{0}C; depicting low energy consumption) in comparison to other catalyst, that needed higher temperature (400 to 500^{0}C), hence high energy consumption.

Table: 4.4 CO activities and hydrogen selectivity & yield of different catalyst

Catalysts	**CO Conversion (%)**	**Temp (°C)**	**H_2 yield (%)**	**Selectivity (%)**	**Stability (hr)**	**Activation Energy (kJ/mol)**	**Ref.**
CuO/CeO_2	78	295	44	98	6	55	Present study
CeO_2	68	295	39	92	6	49	Present study
Ni/Cu/Ce/ Zr/Ca	65	500	55	90	5	99	Oluku et al. [2013]
CuO/CeO_2	67	400	32	99	4	51	Kusar et al. [2006]
Ni/Cu/Ce/ Zr/Gd	45	500	45	98	5	70	Oluku et al. [2013]
Ni/CeO_2-Al_2O_3	95	450	52	73	10	-	Haryanto et al. [2009]
Cu/Ce/Zn	78	400	39	90	5	47	Kusar et al. [2006]

A comparison of CeO_2 nanofiber and composite CuO/CeO_2 nanofiber CO conversion, hydrogen selectivity and hydrogen yield are shown in Figure4.22, Figure4.23 and Figure4.24 respectively. Hydrogen yield and selectivity were maximum: 44% and 99%, respectively at 50% Cu content and stability also give maximum at 50% Cu content (Haryanto et al; 2009). From this figure, it can be observed that increase in the reaction temperature resulted in decrease in CO

conversion and, therefore, H_2 yield (Oluku et al; 2013). The catalyst had CO conversion of 78%, H_2 yield of 44%, and H_2 selectivity of 99%. At the same conditions, the equilibrium CO conversion was 84% with a H_2 yield of 47%. Other researchers have also obtained similar results (Haryanto et al; 2009).

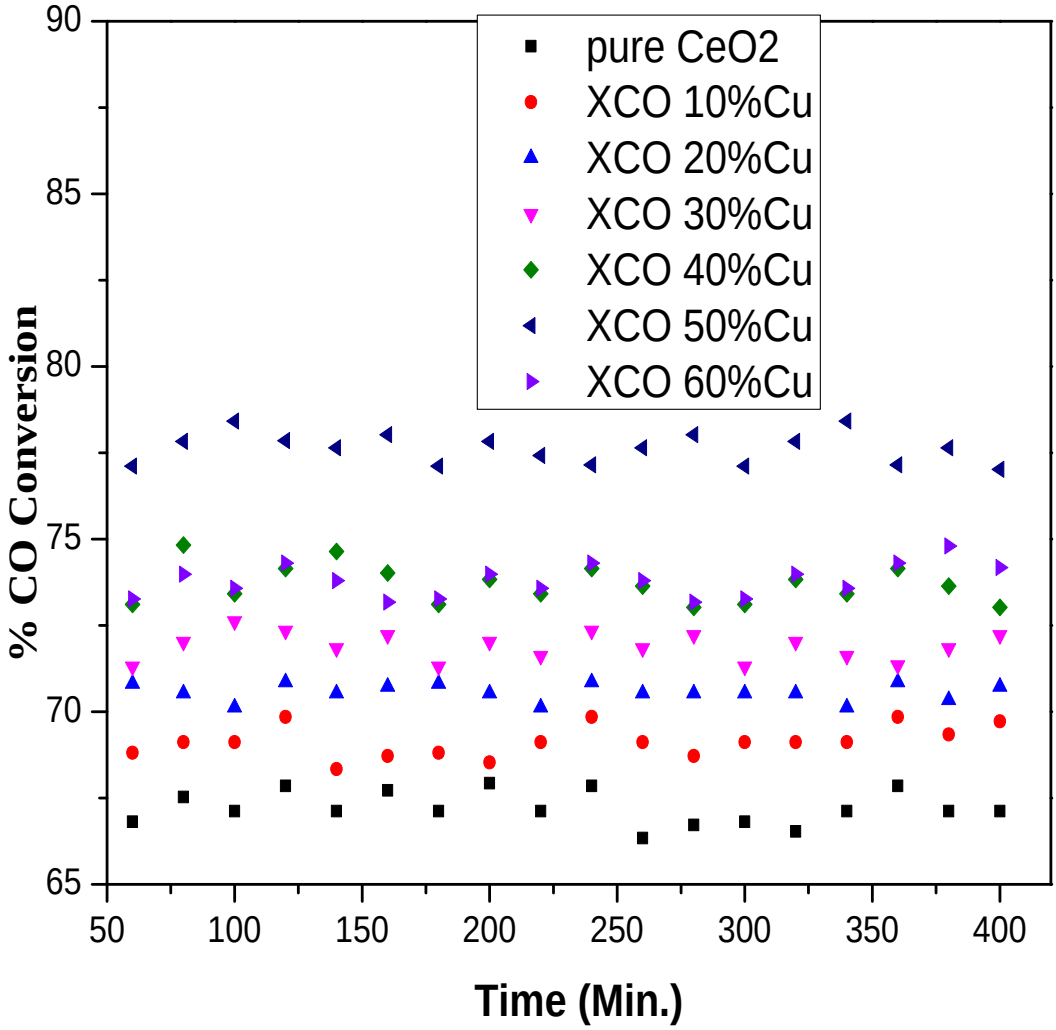

Figure 4.22CO conversion versus time on stream for CeO_2 and composite CuO/CeO_2 nanofiber catalysts at 295°C

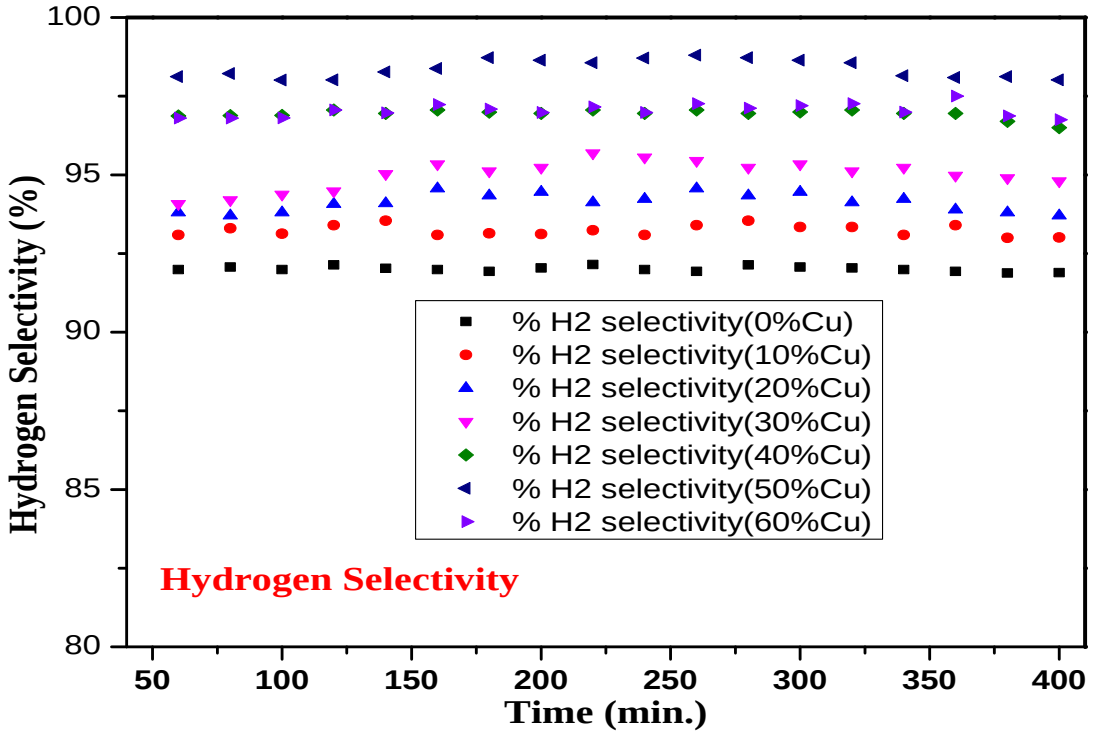

Figure 4.23 Hydrogen selectivity versus time on stream for CeO_2 and composite CuO/CeO_2 nanofiber catalysts at 295°C

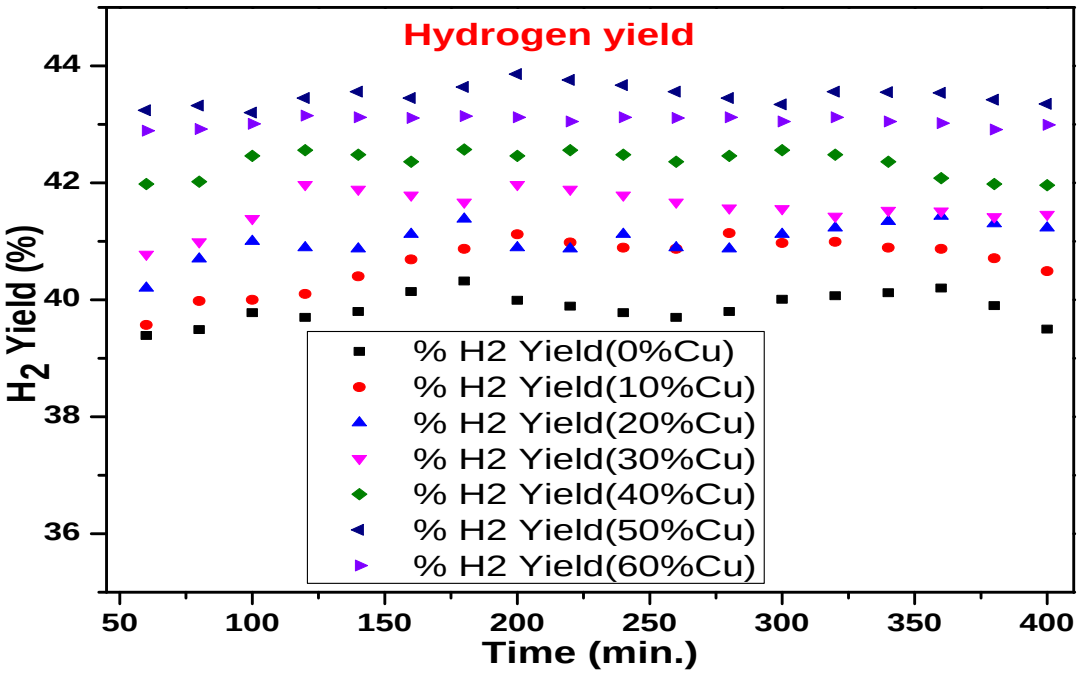

Figure 4.24 Hydrogen yield versus time on stream for CeO_2 and composite CuO/CeO_2 nanofiber catalysts at 295°C

4.1.9 Thermodynamics of Water Gas Shift Reaction:

The water-gas-shift reaction is thermodynamically limited at higher temperatures. The equilibrium constant K is defined in terms of the equilibrium concentrations or partial pressures of the reactants and products as depicted by eqn.4.6.

$$K = \frac{P_{CO2}\,P_{H2}}{P_{CO}\,P_{H2O}} = \frac{X_{CO2}\,X_{H2}}{X_{CO}\,X_{H2O}} = \exp\left(-\frac{\Delta G}{R_{gas}T}\right) \qquad (4.6)$$

The partial pressures may be given in terms of conversion of CO within a reactor and initial feed partial pressure of CO. The equilibrium conversion of CO may be determined from the equilibrium constant as a function of temperature. For example, in the case where equimolar feed of CO and H_2O are fed to the reactor (i.e. $x_{CO} = x_{H2O}$; $x_{H2} = x_{CO2} = 0$), the equilibrium conversion of CO (*X)* can be given by eqn.4.7.

$$X = \frac{\sqrt{K}}{1 + \sqrt{K}} \qquad (4.7)$$

Application of tabulated thermodynamic functions from thermodynamic handbooks provides an expression for ΔG, the Gibbs free energy of the reaction, as a function of temperature (eqn. 4.8) reported by Micro Math, (Math et al; 1998).

$$\Delta G\left(\frac{kj}{mol}\right) = -32.197 + 0.03104T - \frac{1774.7}{T} \qquad (4.8)$$

The equilibrium constant of the reaction (*K*) may be calculated from eqn. 4.9 (Math et al; 1998).

$$\log(K) = -2.4197 + 0.0003855T + \frac{2180.7}{T} \qquad (4.9)$$

4.1.9.1 Kinetics studies: The kinetics of water gas shift reaction was studied over the temperature range of 298-373 K at atmospheric pressure. It is an exothermic reaction. Rate law equation and Arrhenius equation are used for the calculation of the order of reaction and activation energy respectively.

Determination of rate of reaction: The kinetic model for water shift gas reaction is derived from the rate law equation. By using mass balance under plug flow condition, gives

$$F_{CO}dX = -r_{CO}dW \tag{4.10}$$

$$r_{CO} = \frac{dy}{dx} \tag{4.11}$$

Differentiating the polynomial equation obtained between X_A and F_{A0} the value of slope will give the rate of reaction. Plots between X_A and W/F_{A0} were used to calculate the rate of reaction. Where T_1 =35^{0}C, T_2 =45^{0}C, T_3 =65^{0}C, T_4 =85^{0}C and T_5 =105^{0}C.

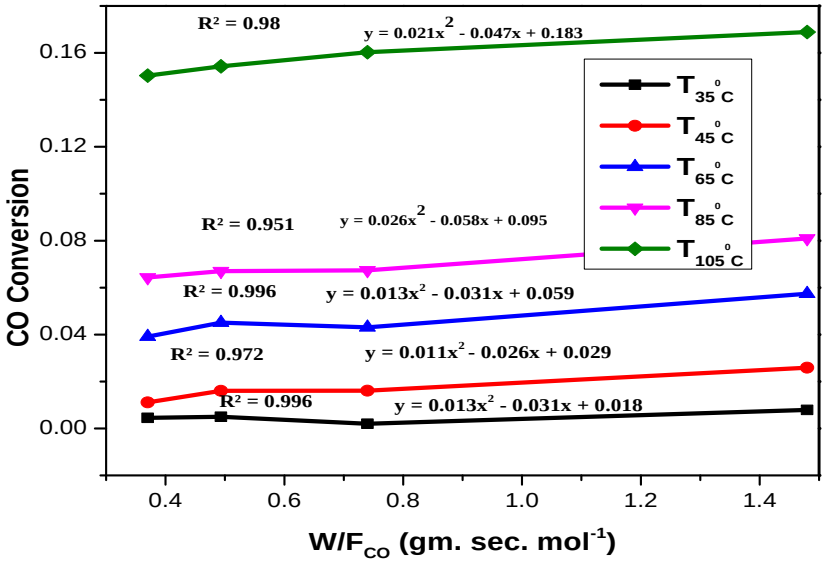

Figure 4.25 Graph between X_{CO} vs W/F_{CO} for water gas shift reaction

Determination of order of reaction: Concentration C_A is calculated using equation:

$$PV = nRT \tag{4.12}$$

$$C_{C0} = \frac{P}{RT} \tag{4.13}$$

$$C_A = C_{A0}(1 - X_{CO}) \tag{4.14}$$

Here t is the time (sec), F_{A0} is flow rate in gmol/litre and V is the volume of reactor (liters). The general rate equation can be written as follows.

$$-r_{CO} = kC_{CO}^{n} \quad (4.15)$$

$$\ln(-r_{CO}) = \ln k + n\ln C_{CO} \quad (4.16)$$

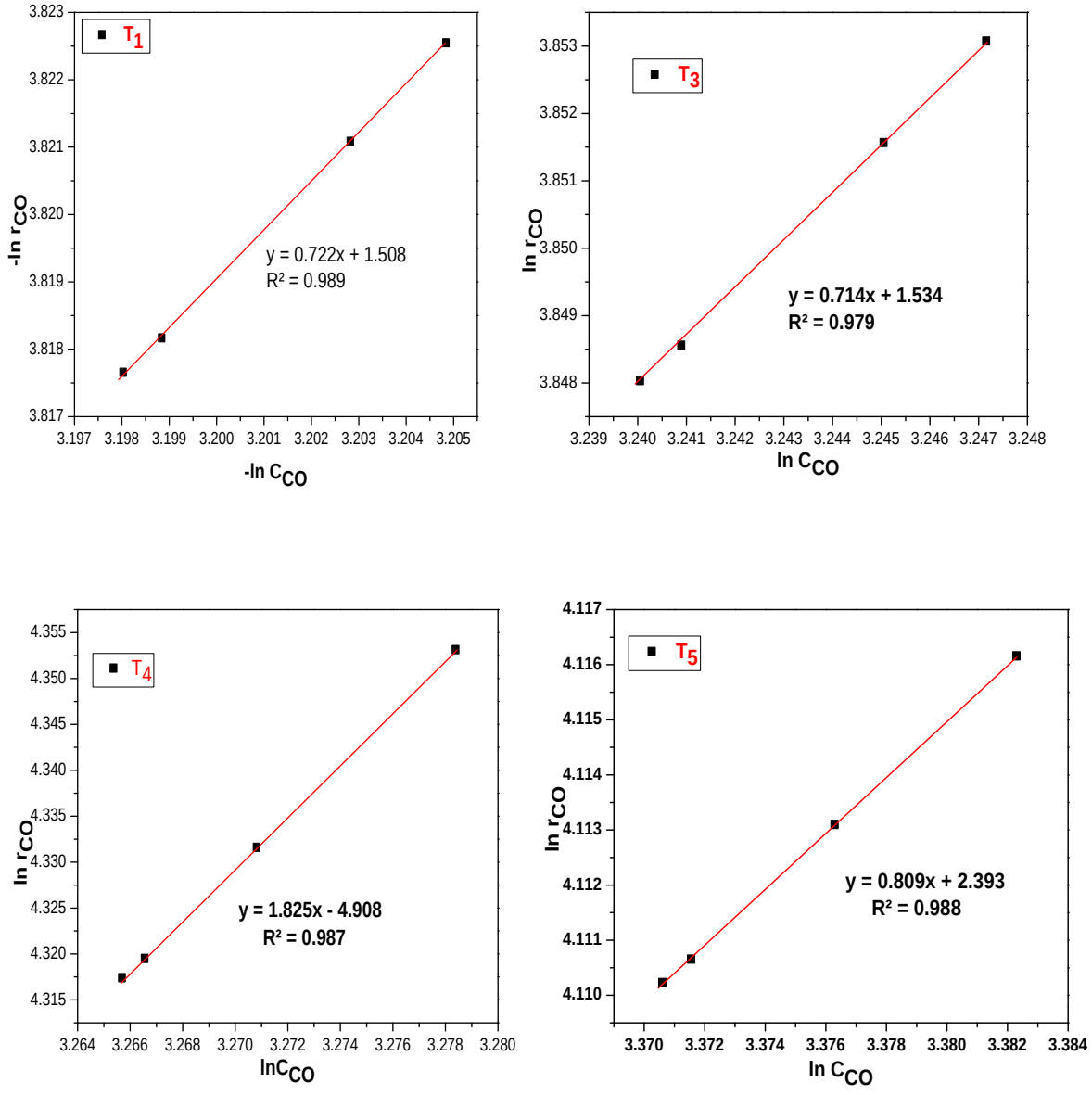

Figure 4.26 Calculation order of reaction for catalytic WGSR at different temperatures

A plot between '$\ln r_A$' vs. '$\ln C_A$' gives a linear relation. The slope of this plot gives the order (n) of the reaction and the intercept, 'lnk' where k is the reaction rate constant. Order of reaction was calculated individually for a range of temperature used in the experiments and then averaged to calculate the overall order of the reaction, which was found to be of first order.

Determination of Activation Energy & Frequency Factor : After calculation of the reaction rate constant 'k' and order of reaction 'n', the activation energy was calculated using Arrhenius equation:

$$K = A\exp(-\frac{E}{RT}) \qquad (4.17)$$

Where, A is the frequency factor, E is the activation energy, R is the universal gas constant and T is the absolute temperature. The kinetic rate constant 'k' is temperature dependence.On taking log of equation 4.17, it can be written as

$$\ln k = \ln A - \frac{E}{RT} \qquad (4.18)$$

The obtained value of k when fitted in equation 4.18 gives a straight line, known as the Arrhenius plot and Figure 4.27 shows the plot between 'lnk' and '1/T', the slope and intercept were calculated to evaluated E and A.

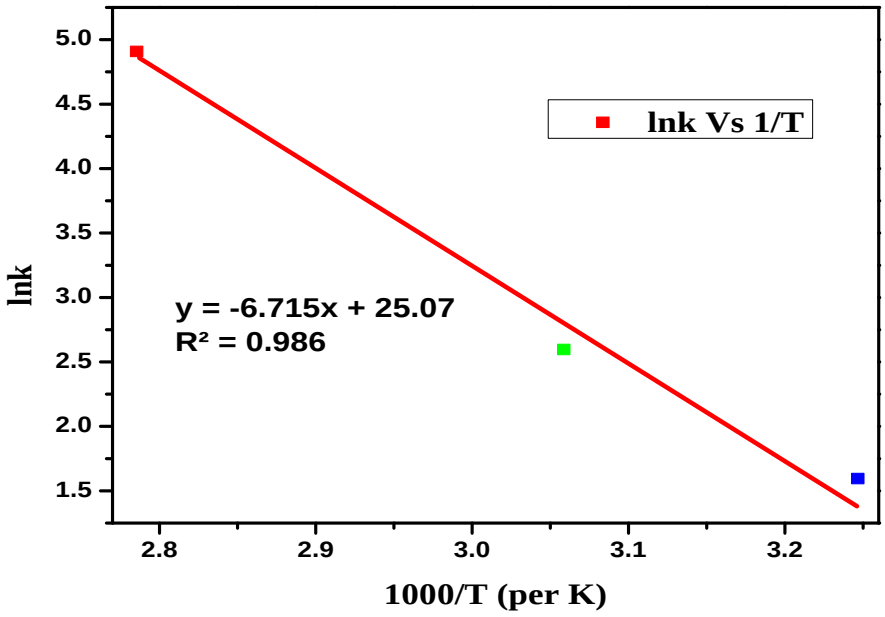

Figure 4.27 Arrhenius plot for water gas shift reaction

The activation energy was found to be E=55 ± 1.37 kJ/mol that is close to the value reported in literature and the error was around 2.5 % of original value of activation energy and error of rate constant was around 4.25% of its original value. Jeong et al. (2015) used the Pt/CeO_2 nano-catalyst prepared by electrospinning method and the lowest activation energy (55 kJ/mol) and the frequency factor A as 6.03x 10^9 sec^{-1}. Weight hourly space velocity of 3816 h^{-1} is found to be optimum under the present experimental conditions. The kinetics of water gas shift reaction over CeO_2 nanofiber and composite CuO/CeO_2 nanofiber catalysts in the temperature range 298-373K represents the following rate expression:

$$\text{Rate of CO} = 6.03X10^9 \frac{55kJ}{RT} C_{CO} \quad mol\ gm_{cat}^{-1} sec^{-1} \tag{4.19}$$

The findings of the study revealed that the ceria nanofiber catalyst has significantly higher surface area and activity at lower energy consumption which will help in effective WGS reaction.